Analysis of hadronic transitions in $\Upsilon(3S)$ decays

F. Butler,[1] X. Fu,[1] G. Kalbfleisch,[1] M. Lambrecht,[1] W. R. Ross,[1] P. Skubic,[1]
J. Snow,[1] P. L. Wang,[1] M. Wood,[1] D. Bortoletto,[2] D. N. Brown,[2] J. Fast,[2] R. L. McIlwain,[2]
T. Miao,[2] D. H. Miller,[2] M. Modesitt,[2] S. F. Schaffner,[2] E. I. Shibata,[2] I. P. J. Shipsey,[2] P. N. Wang,[2]
M. Battle,[3] J. Ernst,[3] H. Kroha,[3] S. Roberts,[3] K. Sparks,[3] E. H. Thorndike,[3] C. H. Wang,[3]
J. Dominick,[4] S. Sanghera,[4] T. Skwarnicki,[4] R. Stroynowski,[4] M. Artuso,[5] D. He,[5] M. Goldberg,[5]
N. Horwitz,[5] R. Kennett,[5] G. C. Moneti,[5] F. Muheim,[5] Y. Mukhin,[5] S. Playfer,[5] Y. Rozen,[5]
S. Stone,[5] M. Thulasidas,[5] G. Vasseur,[5] G. Zhu,[5] J. Bartelt,[6] S. E. Csorna,[6] Z. Egyed,[6]
V. Jain,[6] P. Sheldon,[6] D. S. Akerib,[7] B. Barish,[7] M. Chadha,[7] S. Chan,[7] D. F. Cowen,[7]
G. Eigen,[7] J. S. Miller,[7] C. O'Grady,[7] J. Urheim,[7] A. J. Weinstein,[7] D. Acosta,[8] M. Athanas,[8]
G. Masek,[8] H. Paar,[8] M. Sivertz,[8] A. Bean,[9] J. Gronberg,[9] R. Kutschke,[9] S. Menary,[9]
R. J. Morrison,[9] S. Nakanishi,[9] H. N. Nelson,[9] T. K. Nelson,[9] J. D. Richman,[9] A. Ryd,[9] H. Tajima,[9]
D. Schmidt,[9] D. Sperka,[9] M. S. Witherell,[9] M. Procario,[10] S. Yang,[10] R. Balest,[11] K. Cho,[11]
M. Daoudi,[11] W. T. Ford,[11] D. R. Johnson,[11] K. Lingel,[11] M. Lohner,[11] P. Rankin,[11] J. G. Smith,[11]
J. P. Alexander,[12] C. Bebek,[12] K. Berkelman,[12] D. Besson,[12] T. E. Browder,[12] D. G. Cassel,[12] H. A. Cho,[12]
D. M. Coffman,[12] P. S. Drell,[12] R. Ehrlich,[12] R. S. Galik,[12] M. Garcia-Sciveres,[12] B. Geiser,[12] B. Gittelman,[12]
S. W. Gray,[12] D. L. Hartill,[12] B. K. Heltsley,[12] C. D. Jones,[12] S. L. Jones,[12] J. Kandaswamy,[12] N. Katayama,[12]
P. C. Kim,[12] D. L. Kreinick,[12] G. S. Ludwig,[12] J. Masui,[12] J. Mevissen,[12] N. B. Mistry,[12] C. R. Ng,[12]
E. Nordberg,[12] M. Ogg,[12,*] J. R. Patterson,[12] D. Peterson,[12] D. Riley,[12] S. Salman,[12] M. Sapper,[12]
H. Worden,[12] F. Würthwein,[12] P. Avery,[13] A. Freyberger,[13] J. Rodriguez,[13] R. Stephens,[13] J. Yelton,[13]
D. Cinabro,[14] S. Henderson,[14] K. Kinoshita,[14] T. Liu,[14] M. Saulnier,[14] F. Shen,[14] R. Wilson,[14]
H. Yamamoto,[14] B. Ong,[15] M. Selen,[15] A. J. Sadoff,[16] R. Ammar,[17] S. Ball,[17] P. Baringer,[17]
D. Coppage,[17] N. Copty,[17] R. Davis,[17] N. Hancock,[17] M. Kelly,[17] N. Kwak,[17] H. Lam,[17]
Y. Kubota,[18] M. Lattery,[18] J. K. Nelson,[18] S. Patton,[18] D. Perticone,[18] R. Poling,[18] V. Savinov,[18]
S. Schrenk,[18] R. Wang,[18] M. S. Alam,[19] I. J. Kim,[19] B. Nemati,[19] J. J. O'Neill,[19] H. Severini,[19]
C. R. Sun,[19] M. M. Zoeller,[19] G. Crawford,[20] C. M. Daubenmier,[20] R. Fulton,[20] D. Fujino,[20] K. K. Gan,[20]
K. Honscheid,[20] H. Kagan,[20] R. Kass,[20] J. Lee,[20] R. Malchow,[20] F. Morrow,[20] Y. Skovpen,[20,†]
M. Sung,[20] C. White,[20] J. Whitmore,[20] and P. Wilson[20]

(CLEO Collaboration)

[1]*University of Oklahoma, Norman, Oklahoma 73019*
[2]*Purdue University, West Lafayette, Indiana 47907*
[3]*University of Rochester, Rochester, New York 14627*
[4]*Southern Methodist University, Dallas, Texas 75275*
[5]*Syracuse University, Syracuse, New York 13244*
[6]*Vanderbilt University, Nashville, Tennessee 37235*
[7]*California Institute of Technology, Pasadena, California 91125*
[8]*University of California, San Diego, La Jolla, California 92093*
[9]*University of California, Santa Barbara, California 93106*
[10]*Carnegie-Mellon University, Pittsburgh, Pennsylvania 15213*
[11]*University of Colorado, Boulder, Colorado 80309-0390*
[12]*Cornell University, Ithaca, New York 14853*
[13]*University of Florida, Gainesville, Florida 32611*
[14]*Harvard University, Cambridge, Massachusetts 02138*
[15]*University of Illinois, Champaign-Urbana, Illinois 61801*
[16]*Ithaca College, Ithaca, New York 14850*
[17]*University of Kansas, Lawrence, Kansas 66045*
[18]*University of Minnesota, Minneapolis, Minnesota 55455*
[19]*State University of New York at Albany, Albany, New York 12222*
[20]*Ohio State University, Columbus, Ohio 43210*

(Received 8 July 1993)

Using the CLEO II detector, we have measured the branching fractions for $\Upsilon(3S)\to\pi\pi\Upsilon(1S)$, $\Upsilon(3S)\to\pi\pi\Upsilon(2S)$, and the cascade $\Upsilon(3S)\to\Upsilon(2S)+X$, $\Upsilon(2S)\to\pi^+\pi^-\Upsilon(1S)$, analyzing the exclusive

*Permanent address: Carleton University, Ottawa, Canada K1S 5B6.
†Permanent address: INP, Novosibirsk, Russia.

mode where the daughter Υ state decays to a e^+e^- or $\mu^+\mu^-$ pair, as well as the inclusive $\pi^+\pi^-$ transitions where the final Υ state decays into hadrons. Properties of the $\pi\pi$ system are analyzed. Searches for the cascade decay $\Upsilon(3S)\to\pi^+\pi^- h_b$, $h_b\to\gamma\eta_b$ and $\Upsilon(3S)\to\pi^0 h_b$ were also performed.

PACS number(s): 13.25.Gv, 14.40.Gx

I. INTRODUCTION

The study of the energy levels of heavy quarkonia, their widths and transition amplitudes, is a key tool for modeling the interquark forces and thus provides the experimental basis for solving the theoretical problem of calculating nonperturbative QCD processes [1]. The spectroscopy of the bound $b\bar{b}$ states is particularly rich because of the large number of bound states below the open flavor threshold, and in particular because of the presence of the radial excitations of the spin singlet and triplet S- and P-wave energy levels [2].

The energy levels of the triplet S- and P-wave $b\bar{b}$ states and the electromagnetic and hadronic transitions between them have been studied by the ARGUS [3,4], CLEO [5,6], Crystal Ball [7], and CUSB [8,10,9] Collaborations [11]. The radiative transitions, perhaps the most easily described of these transitions, are dominated by E1 photon emission, and therefore have widths which vary (to lowest order) as $\Gamma\sim|\langle f|r|i\rangle|^2$. Selection rules dictate that there be a change of parity in such E1 decays; consequently decays of the type $\Upsilon(3S)\to\Upsilon(2S)\gamma$ are prohibited. In the absence of relativistic corrections, once the wave functions are known, the widths of, e.g., $\Upsilon(3S)\to\gamma\chi_{bJ}(2P)$ should be immediately calculable. Such decays have recently been studied by both the CUSB [8,10] and the CLEO [6] Collaborations.

Of particular interest for exploring nonperturbative QCD processes are the hadronic transitions between $b\bar{b}$ bound states. These transitions are thought to occur by the emission of at least two gluons, followed by their hadronization. Because of the relatively small mass difference, these gluons are soft and cannot be handled by the perturbative approach to QCD. However, Gottfried [12] suggested that the gluon can be treated in the context of a multipole expansion in $k\cdot r$ of the color field, where k is the gluon momentum and r its position vector; such an approach should be valid for $k\cdot r\ll 1$. For the decay $\Upsilon(3S)\to\Upsilon(2S)+X$, $\langle k\cdot r\rangle$ is of the order of 0.35. The transitions $\psi'\to\pi\pi\psi$ and $\Upsilon(2S)\to\pi\pi\Upsilon(1S)$ have been observed both in the charged and neutral π modes by several groups (see [11] for references) and the $\pi\pi$ mass distribution was found to peak at high mass values. Several authors [13–15] used Gottfried's suggestion and, applying partial conservation of the axial current (PCAC), calculated the partial widths for transitions between $c\bar{c}$ as well as between $b\bar{b}$ states with $\pi\pi$ or η emission. The spectrum of the invariant $\pi\pi$ mass was also calculated in a variety of ways [14–20]; this consistently led to a characteristic peaking of dipion mass at high values, in accord with the available $\psi'\to\pi\pi\psi$ data, and confirmed later in the $\Upsilon(2S)\to\pi\pi\Upsilon(1S)$ transitions. The $\Upsilon(3S)\to\pi\pi\Upsilon(1S)$ and $\Upsilon(3S)\to\pi\pi\Upsilon(2S)$ transitions have also been observed in the $\pi^+\pi^-$ mode [5,9] as well as in the $\pi^0\pi^0$ mode [8,9], but the $\pi\pi$ mass distribution in the $\Upsilon(3S)\to\pi^+\pi^-\Upsilon(1S)$ decay [5,9] shows a double bump behavior that disagrees with those predictions. Several unsuccessful theoretical attempts have been made to remedy this discrepancy by taking into account the known $\pi\pi$ final state interaction [21], or by introducing $\pi\pi$ and/or $\Upsilon\pi$ resonances [16,22]. Lipkin and Tuan [23] suggested that the peculiar behavior of the $\pi\pi$ invariant mass distribution in the $\Upsilon(3S)\to\pi\pi\Upsilon(1S)$ transition is due to coupling to intermediate $B\bar{B}^*$ states, and Moxhay [24] showed that a generic, constant complex amplitude, presumably coupling to virtual $B\bar{B}^*$ states and interfering with the multipole expansion amplitude, could indeed reproduce the experimental $\pi\pi$ mass distribution available at that time.

Zhou and Kuang [25] have performed detailed calculations of the hadronic transitions among triplet S-wave heavy quarkonia, with emission of two pions, taking into account coupled channels effects. In doing so they have written explicitly the amplitude due to intermediate $B\bar{B}^*+\bar{B}B^*$ states. If the B^*'s are triplet S-wave ($b\bar{q}$) states, this is the decay mechanism proposed by Lipkin and Tuan [23] and proportional to $(\mathbf{k}_1\cdot\mathbf{k}_2)$, the dot product of the momenta of the two pions. If the B^*'s are P-wave ($b\bar{q}$) states the amplitude is constant and is consistent with the one used by Moxhay [24]. Zhou and Kuang use the successful unitary quark model [26], the quark pair creation mechanism of Le Yaouanc *et al.* [27] and a well tested nonrelativistic potential shape to write an amplitude with no arbitrary constants, except the magnitude and phase of the multipole expansion term, that they obtain from experiment, fitting $d\Gamma/dm_{\pi\pi}$ for the $\psi'\to\psi\pi\pi$ transition [4]. Their model predicts $\pi\pi$ decay rates larger than those calculated by Kuang and Yan [13] and in closer agreement with the experimental ones. It also successfully predicts tiny differences between the shapes of $d\Gamma/dm_{\pi\pi}$ for the $\psi'\to\psi\pi\pi$ and the $\Upsilon(2S)\to\Upsilon(1S)\pi\pi$. However, according to their model, the term in the amplitude due to the $B\bar{B}^*+\bar{B}B^*$ intermediate states turns out to be at least one order of magnitude smaller than the multipole expansion term and thus inconsistent both with the experimental $m_{\pi\pi}$ distribution in $\Upsilon(3S)\to\Upsilon(1S)\pi\pi$ decay and with Moxhay's interpretation of the low $m_{\pi\pi}$ bump effect. Zhou and Kuang also show that using the Cornell coupled channel model [28], the effect of the $B\bar{B}^*+\bar{B}B^*$ intermediate state would be even smaller. We report here new, higher statistics measurements of the decay branching fractions of the $\Upsilon(3S)\to\pi\pi\Upsilon(1S/2S)$ transitions and their $\pi\pi$ mass distributions in both the $\pi^0\pi^0$ and $\pi^+\pi^-$ modes. We have also similarly analyzed the $\Upsilon(2S)\to\pi^+\pi^-\Upsilon(1S)$ transition. Isospin conservation, after taking phase space differences into account, precisely relates the branching fractions of the $\pi^+\pi^-$ and $\pi^0\pi^0$ modes in these transitions.

The final states containing a $\pi^+\pi^-$ pair and those containing a $\pi^0\pi^0$ pair require analysis procedures that are very different and largely independent; they rely mostly on different components of the CLEO II detector and are subject to different systematic errors and bias. The analysis involving $\pi^0\pi^0$ pairs is largely based on information extracted from the CsI electromagnetic shower detector and uses only events with the daughter Υ decaying in a e^+e^- or $\mu^+\mu^-$ pair ("exclusive" analysis). The CLEO II tracking devices provide most of the information needed for the analysis of the final states involving $\pi^+\pi^-$ pairs. This analysis consists of an "exclusive" analysis, as above, and an analysis that uses the more copious, higher multiplicity, daughter Υ decay modes ("inclusive" analysis). The two analyses based respectively on $\pi^0\pi^0$ and $\pi^+\pi^-$ pairs, because of their complexity, thus warrant separate descriptions. On the other hand, because of their complementarity, they support each other and, in a final section, we draw common conclusions and compare our results with previous ones.

In the bottomonium system, according to present models, several other states must exist and their observation is necessary to complete the heavy quark picture. Among them is the $^1P_1$, designated as h_b. We report here a search for the transition $\Upsilon(3S)\to\pi^+\pi^-h_b$ and give an upper limit for the corresponding decay branching ratio.

Because of the complexity of this paper, it is appropriate to give here a table of contents that begins with the next section.

II. DATA SAMPLE AND THE CLEO II DETECTOR

We use the CLEO II detector [29] at the Cornell Electron Storage Ring (CESR) to observe the decays of the $\Upsilon(3S)$ produced in e^+e^- annihilation. The data sample consists of 130 pb^{-1} of integrated luminosity taken near the peak of the $\Upsilon(3S)$ resonance. The number of $\Upsilon(3S)$ resonant decays produced in this sample is $N_{3S}^{\rm pro}=(465\pm31)\times10^3$.

Charged particles are tracked in a 1.5 Tesla magnetic field through three concentric cylindrical drift chambers covering 94% of the solid angle. The innermost chamber is a six-layer straw tube vertex detector of inner radius 4.5 cm with 95 μm position accuracy in the r-ϕ plane. It is followed by a ten-layer pressurized inner drift chamber vertex detector with a position accuracy of 100 μm in r-ϕ. The main cylindrical drift chamber [30] contains 51 anode layers, 11 of which are strung at angles of 1.9° to 3.5° to the z axis. It has a position accuracy of 120 μm in r-ϕ and dE/dx resolution (measured on Bhabha scattering events) of 6.5% for particle identification. The outer radius of the main drift chamber is 1 m. Cathode layers are located at the inner and outer radii of the ten-layer inner drift chamber, and at the inner and outer radii of the main drift chamber. Time-of-flight counters with 160 ps resolution are located outside the drift chambers.

Photon and π^0 detection as well as electron identification use the CsI electromagnetic shower detector [31]. It consists of 7800 CsI(Tl) crystals between the time-of-flight counters and the superconducting magnet coil in the barrel region and, in the forward regions, between the drift chamber plates and the magnet pole pieces, altogether covering 95% of the solid angle. Each barrel crystal is 30 cm (16.2 radiation lengths) long and roughly trapezoidal in shape, tapering to 5×5 cm^2 on the end toward the interaction region; they point approximately toward the interaction region. The endcap crystals are rectangular parallelepipeds of approximately the same size as the barrel crystals, with their axes parallel to the beam direction. The material in the drift chamber endplates, electronics, and cables degrades the performance of the calorimeter in the endcaps, especially at the two ends of the barrel region. Because of that, in some critical cases we limit our acceptance to the "good barrel" region of the calorimeter covering the angular region $|\cos\theta|<0.707$. The energy calibration [6] makes use of Bhabha scattering and radiative Bhabhas as well as $e^+e^-\to\gamma\gamma$ reactions and $\pi^0\to\gamma\gamma$ decays. For the low multiplicity final states, the energy resolution in the "good barrel" portion of the calorimeter varies from 3.7% at 100 MeV to 1.2% at 5 GeV.

Muons are identified by their penetration in the three 36 cm thick slabs of iron that surround the superconducting coil in an octagonal geometry, and in the iron pole pieces of the magnet. The detection [32] is provided by three superlayers of counters, one after each slab of iron, and a superlayer on each endcap. Each superlayer consists of three layers of "plastic streamer tubes," operated in the proportional mode.

In order to estimate detection efficiencies for the reactions studied, we generate Monte Carlo events in the desired channels using the JETSET 7.3 package. The events are then processed through a GEANT-based [33] CLEO II simulation package and reconstructed and analyzed as real data.

III. THE $\pi^0\pi^0$ ANALYSIS

A. $\Upsilon(3S)\to\pi^0\pi^0\Upsilon(1S/2S)$ transitions

We study the following transitions in the exclusive mode where the daughter Υ states decay into l^+l^- lep-

ton pairs (l represents either an e or a μ):

$$\Upsilon(3S)\to\Upsilon(2S)\pi^0\pi^0 \quad \Upsilon(2S)\to l^+l^- \ , \tag{1}$$

$$\Upsilon(3S)\to\Upsilon(1S)\pi^0\pi^0 \quad \Upsilon(1S)\to l^+l^- \ . \tag{2}$$

We select events with $\Upsilon(1S/2S)\to l^+l^-$ decays by requiring two oppositely charged lepton tracks, each with momentum $|p_l|>4.0$ GeV. The electron channel events are triggered through the trigger lines designed for Bhabha events. These lines are heavily prescaled in the endcap region. In order to avoid these regions, we require that each electron be within the fiducial region of the barrel time-of-flight counters ($|\cos\theta_l|<0.707$, where θ_l is the angle of either lepton to the beam axis). In what follows, we apply the same angular cut for the muon channel as well.

The lepton tracks must form an opening angle greater than 170°. Electrons are identified by requiring that the track ionization be consistent with the electron hypothesis, that an electromagnetic shower be associated with the track, and that the ratio E/p between the shower energy and the magnitude of the track momentum measured in the central detector be close to 1, within momentum dependent limits derived from the respective resolutions. Muons are identified by requiring that the track be associated with a "shower" of energy consistent with a minimum ionizing track (100 to 400 MeV) and that they penetrate at least three nuclear absorption lengths of the iron absorber.

To select $\pi^0\pi^0$ transitions, we require that there be at least four photon showers in the CsI calorimeter, and that each π^0 have at least one photon shower in the "good barrel" portion of the calorimeter ($|\cos\theta|<0.707$). Showers are considered to be photon candidates if they have an energy greater than 30 MeV and if they have the narrow lateral energy distribution characteristic of an isolated electromagnetic shower. As a measure of this lateral energy distribution, we use the fraction of the energy deposited in the central 3×3 matrix of crystals relative to the central 5×5 matrix of crystals.

These photons can be paired in different ways to make two π^0's. A photon pair is considered to be a π^0 candidate if the invariant mass is within 30 MeV of the known π^0 mass. In order to determine the goodness of a pairing, the mass of one pair of photons is plotted against that of the other pair. We take the best pairing to be the one with the minimum Cartesian distance between the point given by the masses of the two photon pairs and the point corresponding to two π^0's of nominal mass. The pairs of photons are kinematically fitted to the known π^0 mass if they make a mass combination within 2.58 σ of the π^0 mass (where σ, the π^0 mass resolution, is about 5 MeV but depends on the energies of the photons and their locations in the detector). We define $m_m(\pi\pi)$, the missing mass of the $\pi\pi$ system, as

$$m_m(\pi\pi)\equiv\sqrt{(2E_b-E_{\pi^1}-E_{\pi^2})^2-(\mathbf{p}_{\pi^1}+\mathbf{p}_{\pi^2})^2} \tag{3}$$

where E_b is the beam energy and E_{π^i} and $\mathbf{p}_{\pi^i}$ are the measured energies and momenta of the two pions. In Fig. 1 we plot the l^+l^- invariant mass $m(l^+l^-)$ vs $m_m(\pi^0\pi^0)$. Clean signals are evident at the masses of the $\Upsilon(1S)$ (9.460 GeV) and $\Upsilon(2S)$ (10.023 GeV). The rectangular shape of the signal regions is due to the vastly superior resolution in $m_m(\pi^0\pi^0)$. A clustering of points can also be seen in the band $m(l^+l^-)\sim m(\Upsilon(1S))$ at $m_m(\pi^0\pi^0)\sim m(\Upsilon(2S))$ and ~9.80 GeV. These are due, respectively, to the cascade reactions

$$\Upsilon(3S)\to\Upsilon(2S)\pi^0\pi^0 \ , \quad \Upsilon(2S)\to\Upsilon(1S)+\text{"undetected"} \ , \quad \Upsilon(1S)\to l^+l^- \ , \tag{4}$$

and

$$\Upsilon(3S)\to\Upsilon(2S)+\text{"undetected"} \ , \quad \Upsilon(2S)\to\Upsilon(1S)\pi^0\pi^0 \ , \quad \Upsilon(1S)\to l^+l^- \ , \tag{5}$$

where the photons or very low energy charged pions ("undetected") from one of the transitions are either undetected or not used in the analysis. The cluster at $m_m(\pi^0\pi^0)=m(\Upsilon(2S))$ and $m(l^+l^-)=m(\Upsilon(1S))$ is due to the cascade decay (4) and the one at $m_m(\pi^0\pi^0)\sim9.80$ GeV is due to the $\Upsilon(2S)\to\Upsilon(1S)\pi^0\pi^0$ transition in cascade decay (5), where $m_m(\pi^0\pi^0)$ has been miscalculated by taking the $\Upsilon(3S)$ as the initial state. By selecting events with no additional photon showers or charged tracks, we have verified that these two additional regions

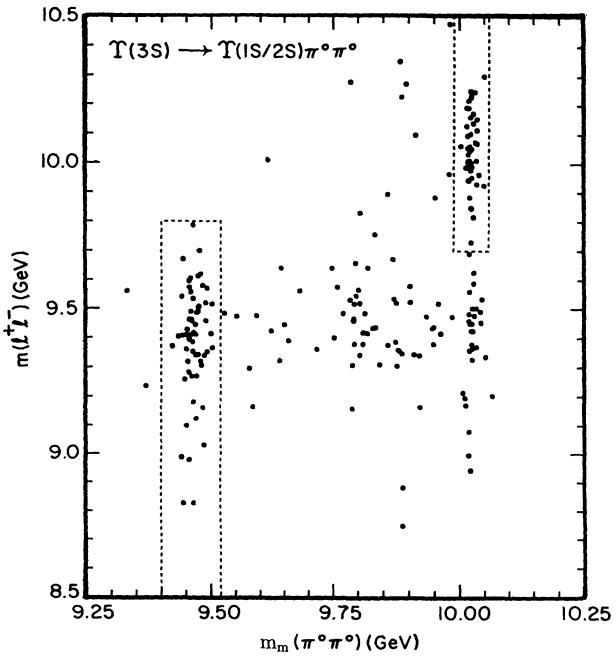

FIG. 1. Plot of the dilepton invariant mass $[m(l^+l^-)]$ vs the missing mass of the $\pi^0\pi^0$ system ($m_m(\pi^0\pi^0)$). The dashed boxes show the signal regions.

become much less populated. Most of the few remaining background points in Fig. 1 are due to mispairing of photon showers from the cascade reactions above.

We select $\Upsilon(3S)\to\pi^0\pi^0\Upsilon(2S)$ decays by counting events in the region $9.7<m(l^+l^-)<11.4$ GeV, $9.99<m_m(\pi^0\pi^0)<10.06$ GeV as shown in Fig. 1. Similarly, we select $\Upsilon(3S)\to\pi^0\pi^0\Upsilon(1S)$ decay by counting events in the region $8.5<m(l^+l^-)<9.8$ GeV, $9.40<m_m(\pi^0\pi^0)<9.52$ GeV. The $m_m(\pi^0\pi^0)$ distributions in the region $9.7<m(l^+l^-)<11.4$ GeV and in the region $8.5<m(l^+l^-)<9.8$ GeV are shown in Figs. 2(a) and 2(b), respectively. We estimate the small background under the peaks of the individual and combined electron and muon sample in the following way. For the $\Upsilon(3S)\to\pi^0\pi^0\Upsilon(1S)$ transition we fit the $m_m(\pi^0\pi^0)$ distribution with a skewed Gaussian for the signal and a linear background in the region $9.30<m_m(\pi^0\pi^0)<9.70$ GeV. For the $\Upsilon(3S)\to\pi^0\pi^0\Upsilon(2S)$ transition, we fit the signal with a symmetric Gaussian and a linear background in the region $9.90<m_m(\pi^0\pi^0)<10.10$ GeV. The results of the fits are given in Table I and shown in Fig. 2 for the combined electron and muon sample. The combined branching ratio is the weighted average of the results from the electron and muon channels.

In order to estimate detection efficiencies for the reactions studied, Monte Carlo $\Upsilon(3S)\to\pi^0\pi^0\Upsilon(1S/2S)$ events are generated with a $(1+\cos^2\theta_l^*)$ (where θ_l^* is the angle either lepton makes with the beam direction in the rest frame of the daughter Υ state) distribution assumed for the lepton pair [as expected if the dipion system carries away no angular momentum and consistent with ARGUS [34] measurements for $\Upsilon(2S)\to\pi^+\pi^-\Upsilon(1S)$]. The events are then processed through a GEANT-based CLEO II simulation package and reconstructed and analyzed as real data. There is good agreement between data and Monte Carlo simulation in the π^0 mass resolution, the dilepton invariant mass resolution, the π^0 momentum spectrum, the photon energy spectrum, and the $\pi^0\pi^0$ recoil mass resolution. The trigger efficiency for e^+e^- channel events is nearly 100% because these events satisfy the Bhabha trigger settings which are designed to have very high efficiency. We estimate the $\mu^+\mu^-$ channel trigger efficiency by studying the observed Bhabha and dimoun cross sections in $e^+e^-\to l^+l^-$ events. We calculate the effect of the additional photons in the event in enhancing the $\mu^+\mu^-$ channel trigger efficiency and obtain a value (82±1)% for $\Upsilon(3S)\to\pi^0\pi^0\Upsilon(1S)\to\pi^0\pi^0\mu^+\mu^-$ and (80±2)% for $\Upsilon(3S)\to\pi^0\pi^0(2S)\to\pi^0\pi^0\mu^+\mu^-$. The slightly lower efficiency in the $\Upsilon(2S)$ case is because of the lower energy of the additional photons. The efficiencies reported in Table I include these trigger efficiencies.

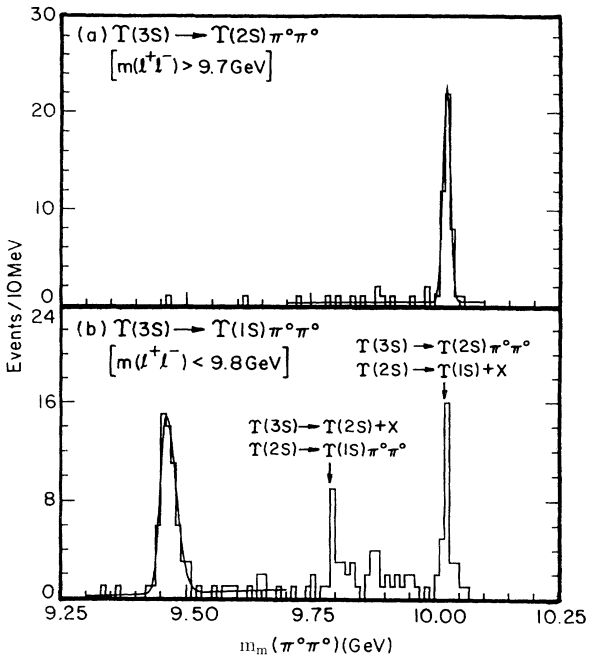

FIG. 2. Missing mass $m_m(\pi^0\pi^0)$ distributions for (a) $\Upsilon(3S)\to\pi^0\pi^0\Upsilon(2S)$ $[m(l^+l^-)>9.7$ GeV], and (b) $\Upsilon(3S)\to\pi^0\pi^0\Upsilon(1S)$ $[m(l^+l^-)<9.8$ GeV]. The curves overlayed on the histograms are the fits to the signal and background as described in the text.

The branching ratios for reactions (1) and (2) are calculated as follows:

$$\mathcal{B}(\Upsilon(3S)\to\pi^0\pi^0\Upsilon(nS))=\frac{(N_{l^+l^-}/\epsilon_{nS})}{N_{3S}^{\rm pro}\times\mathcal{B}(\Upsilon(nS)\to l^+l^-)}$$

where $N_{3S}^{\rm pro}$, the number of resonant $\Upsilon(3S)$ produced, has been previously given and $N_{l^+l^-}$ and the Monte Carlo efficiencies ϵ_{nS} are shown in Table I. We use the following values [11] for the leptonic decay branching ratios of the daughter Υ states:

$$B(\Upsilon(1S)\to l^+l^-)=2\mathcal{B}(\Upsilon(1S)\to\mu^+\mu^-)=(4.96\pm0.12)\%$$

and

TABLE I. Branching ratios for exclusive $\Upsilon(3S)\to\pi^0\pi^0\Upsilon(1S/2S)$ decays in which $\Upsilon(1S/2S)\to l^+l^-$ is reconstructed.

Decay	Mode	Yield	Eff. (%)	Branching ratio (%)
$\Upsilon(3S)\to\pi^0\pi^0\Upsilon(1S)$	$\mu^+\mu^-$	24.9±5.1	11.9±0.4	1.82±0.38±0.16±0.04
	e^+e^-	31.6±5.9	12.4±0.4	2.21±0.42±0.20±0.05
	l^+l^-			1.99±0.28±0.18±0.05
$\Upsilon(3S)\to\pi^0\pi^0\Upsilon(2S)$	$\mu^+\mu^-$	25.7±5.1	11.9±0.4	3.53±0.71±0.39±0.57
	e^+e^-	15.5±4.4	11.8±0.4	2.15±0.62±0.22±0.35
	l^+l^-			2.75±0.47±0.29±0.44

$$\mathcal{B}(\Upsilon(2S)\to l^+l^-)=2\mathcal{B}(\Upsilon(2S)\to\mu^+\mu^-)$$
$$=(2.62\pm0.42)\% \ .$$

In Table I, the first error in the branching ratios is statistical, the second is the systematic error from this analysis. The third error is due to the uncertainty in the leptonic decay branching ratios of $\Upsilon(2S)$ and $\Upsilon(1S)$.

B. The $\pi^0\pi^0$ invariant mass spectra

Since the background under the narrow $\Upsilon(1S/2S)$ peaks is small, we obtain the $\pi^0\pi^0$ invariant mass distributions for the two transitions by selecting the events in the respective regions of the $m(l^+l^-)$ vs $m_m(\pi^0\pi^0)$ plot as shown in Fig. 1. The detection efficiency, obtained from the Monte Carlo simulation, is largely independent of $m(\pi^0\pi^0)$.

The efficiency corrected $\pi^0\pi^0$ invariant mass spectra for the transitions $\Upsilon(3S)\to\pi^0\pi^0\Upsilon(1S)$ and $\Upsilon(3S)\to\pi^0\pi^0\Upsilon(2S)$ are shown in Fig. 3 [35]. The dipion spectrum for $\Upsilon(3S)\to\pi^0\pi^0\Upsilon(1S)$ decay is consistent with the peculiar double peak structure observed in charged pion transitions. Also the spectrum for the $\Upsilon(3S)\to\pi^0\pi^0\Upsilon(2S)$ decay agrees with that of the charged pion transition in showing the high mass enhancement consistent with the multipole expansion model.

We fit the $m(\pi^0\pi^0)$ distributions to three representative models and give the results in Fig. 3. The continuous line is the best fit to the simple expression [14–20]

$$\frac{d\Gamma}{dm_{\pi\pi}}=|A|^2|m^2_{\pi\pi}-m^2_{\pi}|^2\frac{d(X_{\rm PS})}{dm_{\pi\pi}} \ , \qquad (6)$$

the dashed line is the fit to the Bélanger *et al.* model [21], and the dot-dashed line to the Moxhay model [24].

In the $\Upsilon(3S)\to\pi^0\pi^0\Upsilon(1S)$ decay, the excess in the low mass region produces a poor fit to Eq. (6) [χ^2/(degrees of freedom)=24/9]. Bélanger *et al.* [21] took into account the $\pi\pi$ S-wave final state interaction but that does not produce a low mass peak either [χ^2/(degrees of freedom)=22/9]. Moxhay [24] proposed a simple parametrization of the possible effect of intermediate $B\bar{B}^*$, $B^*\bar{B}$ states [23] by adding a constant, complex term to the Bélanger *et al.* amplitude, according to the equation:

$$\frac{d\Gamma}{dm_{\pi\pi}}=|A|^2|m^2_{\pi\pi}F(m^2_{\pi\pi})-(B/A)|^2\frac{d(X_{\rm PS})}{dm_{\pi\pi}} \qquad (7)$$

where $F(m^2_{\pi\pi})$ is the amplitude of Bélanger *et al.* As shown in Fig. 3, this model gives an acceptable fit (χ^2/degrees of freedom)=6.4/7) of the $\pi^0\pi^0$ mass distributions, with parameters $\mathrm{Re}(B/A)=0.12\pm0.02$ and $\mathrm{Im}(B/A)=0.26\pm0.02$.

The dipion invariant mass spectrum for the $\Upsilon(3S)\to\pi^0\pi^0\Upsilon(2S)$ transition agrees with the multipole expansion model prediction of peaking only at high mass [χ^2/degrees of freedom)=4.1/9]. The other two models give very similar distributions.

C. Search for $\Upsilon(3S)\to\pi^0h_b$

An inclusive search is performed for the decay $\Upsilon(3S)\to\pi^0h_b\to$hadrons. This decay should result in a monochromatic π^0. In Fig. 4, we plot the mass of a single π^0 recoiling against the $\Upsilon(3S)$, (i.e., $\sqrt{M^2_{\Upsilon(3S)}-E^2_{\pi^0}-p^2_{\pi^0}}$). For an h_b mass at the spin-weighted average of the χ_b triplet, we should see a signal at 9.9 GeV in this plot. We fit the data points to a smooth background and a Gaussian signal shape with the

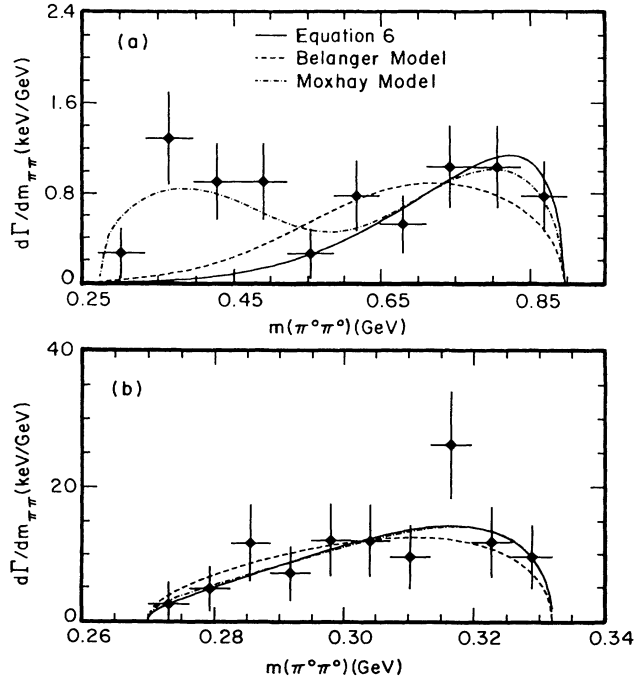

FIG. 3. Efficiency corrected dipion invariant mass $m(\pi^0\pi^0)$ spectra for (a) $\Upsilon(3S)\to\pi^0\pi^0\Upsilon(1S)$ and (b) $\Upsilon(3S)\to\pi^0\pi^0\Upsilon(2S)$.

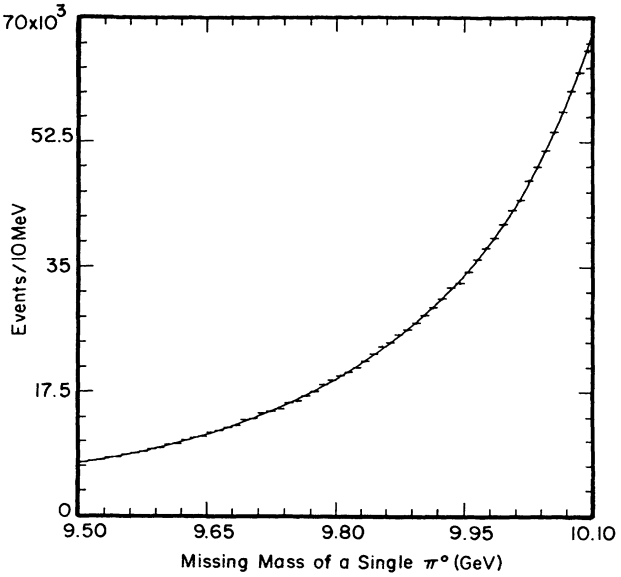

FIG. 4. Search for $\Upsilon(3S)\to\pi^0h_b$. The solid line is a fit to the data points.

mean fixed at the expected value and the width fixed to the π^0 mass resolution (6 MeV) and obtain a yield of -275 ± 270. We vary the mean of the Gaussian between 9.89 GeV and 9.91 GeV in steps of 1 MeV in order to scan for the h_b and see that the yield is consistently around -250 ± 250. The π^0 finding efficiency in an hadronic environment is 35%. The 90% confidence level upper limit on the branching ratio $\mathcal{B}(\Upsilon(3S)\to\pi^0 h_b)$ calculated from these numbers is 0.27%.

IV. THE $\pi^+\pi^-$ ANALYSIS

We study the following transitions in the exclusive mode where the daughter Υ state decays to e^+e^- or $\mu^+\mu^-$ pairs and in the inclusive mode where the daughter Υ state decays hadronically:

(1) $\Upsilon(3S)\to\pi^+\pi^-\Upsilon(1S)$.

(2) $\Upsilon(3S)\to\pi^+\pi^-\Upsilon(2S)$.

(3) $\Upsilon(3S)\to\Upsilon(2S)+X, \Upsilon(2S)\to\pi^+\pi^-\Upsilon(1S)$,

where we assume X is either $\pi^+\pi^-$, $\pi^0\pi^0$, or $\gamma\gamma$.

The observed momentum spectra of the charged pions is shown in Fig. 5. Because of the broad range of momenta covered, cuts are tailored for each transition, separately for the exclusive and inclusive modes, in order to maximize the sensitivity in each transition. The average measured distance of closest approach to the beam axis (DOCA) increases with decreasing pion momentum and we must use momentum dependent DOCA cuts.

Each $\pi^+\pi^-$ missing mass distribution from the data and Monte Carlo simulation is fit with a Gaussian distribution for the signal and a third-order polynomial for the background. The signals are also fit with asymmetric Gaussians to test the sensitivity of the area measurement to a different signal shape. The sensitivity of the area measurement to changes in background shape is tested by varying the extent of the fitting region. The variations in area measurement from different signal shapes and background shapes are incorporated into the systematic uncertainty. The accuracy of the Monte Carlo simulation is checked by studying the consistency between the data and Monte Carlo in the observables of these decays such as missing mass resolutions, decay angle distributions, and charged pion momentum spectra.

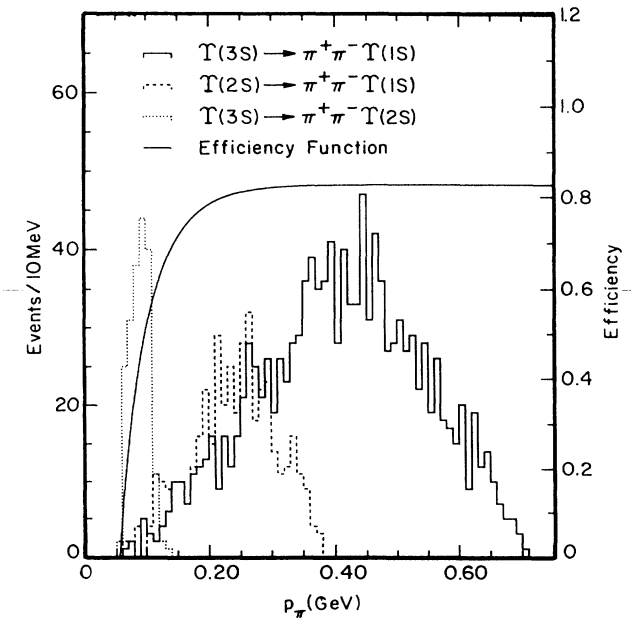

FIG. 5. Observed pion momentum spectra for $\Upsilon(3S)\to\pi^+\pi^-\Upsilon(1S)$, $\Upsilon(3S)\to\pi^+\pi^-\Upsilon(2S)$, and $\Upsilon(2S)\to\pi^+\pi^-(1S)$ candidates (track count is shown with the scale on the left). The dependence of charged particle detection efficiency on particle momentum is also shown (with scale on the right).

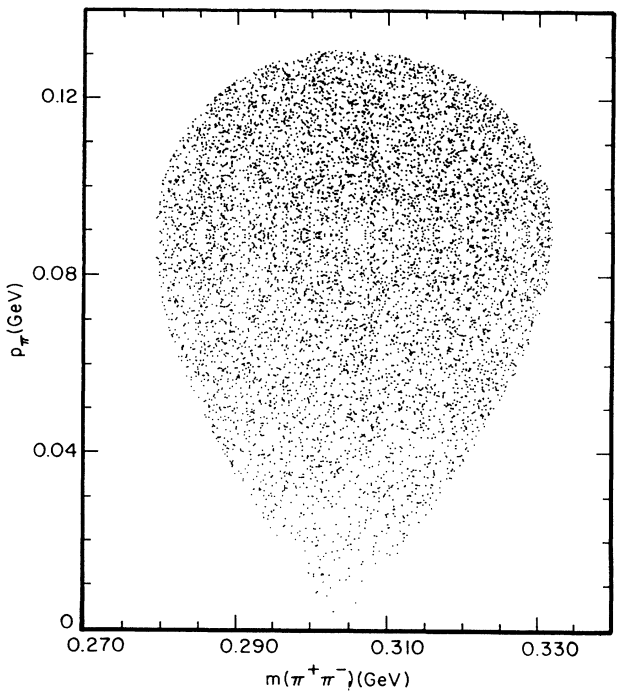

FIG. 6. Scatter plot of charged pion momentum vs $\pi^+\pi^-$ invariant mass (two entries per event) for $\Upsilon(3S)\to\pi^+\pi^-\Upsilon(2S)$ using our Monte Carlo generator for this process.

The distributions of the $\pi^+\pi^-$ missing mass for each dipion invariant mass bin are fit (with mean and width of the signal function fixed according to the values obtained from Monte Carlo simulations). This provides the $\pi^+\pi^-$ invariant mass distribution for each transition. The Monte Carlo simulation is used to determine the dipion efficiency as a function of invariant mass. A phase space distribution of pion momentum versus dipion invariant mass shows that the greatest momentum spread occurs at the central value of invariant mass, as shown in Fig. 6. The efficiency functions are fairly symmetric about the central value and are smoothed by making a fit assuming an $a+bx^2$ dependence on the invariant mass. The invariant mass distributions from data are corrected using efficiencies from the fitting function.

A. Exclusive event selection

Only the $\Upsilon(1S,2S)\to e^+e^-,\mu^+\mu^-$ decays are considered here. Candidate exclusive events are therefore

selected by requiring two oppositely charged tracks, each with momentum $|\mathbf{p}| > 3.5$ GeV and 2 to 5 charged tracks with $|\mathbf{p}| < 750$ MeV. The low momentum tracks are assumed to be charged pions and are required to have specific ionization in the main drift chamber within 3 standard deviations (σ) of that expected for a pion. Each lepton is required to be within the fiducial region of the barrel time-of-flight counters ($|\cos\theta_l| < 0.7$, where θ_l is the angle of either lepton with respect to the beam axis).

Figure 7(a) shows the exclusive dipion missing mass distribution. Bhabha events with a converted radiated photon are the primary source of background. Figure 7(b) shows the $\pi^+\pi^-$ missing mass spectrum with basic cuts applied to try to eliminate the large background (the angle between the direction of the dipion system and the nearest lepton is required to be greater than 0.1 radian; the quadratic sum of the DOCA of the pions must be less than 2 cm). The $\Upsilon(2S)\to\pi^+\pi^-\Upsilon(1S)$ mass peak is shifted from the $\Upsilon(1S)$ mass by the mass difference between the $\Upsilon(3S)$ and $\Upsilon(2S)$, about 330 MeV, since the assumption that these pions are direct decay products of the $\Upsilon(3S)$ is incorrect.

As we discussed in Sec. III A we expect a $(1+\cos^2\theta_l^*)$ distribution with respect to the beam axis for the lepton pair from the decay of $\Upsilon(1S)$ and $\Upsilon(2S)$ if the dipion system carries away no angular momentum. Using the $\Upsilon(3S)\to\pi^+\pi^-\Upsilon(1S)$ missing mass as a tag of events with leptons from the $\Upsilon(1S)$, this $\cos\theta_l^*$ dependence can be verified as shown in Fig. 8. The fit confirms the assumption that the leptons have a $(1+\cos^2\theta_l^*)$ distribution with a 65% confidence level, consistent with the expectation

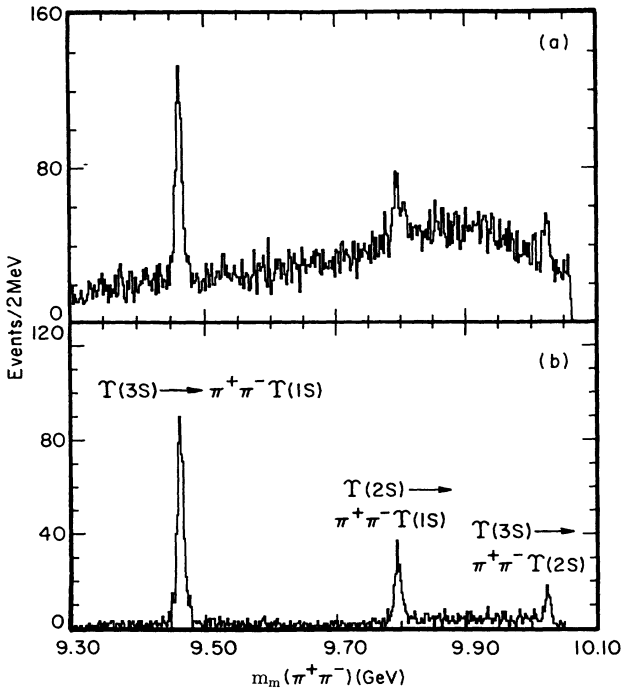

FIG. 7. (a) Exclusive $\pi^+\pi^-$ missing mass. (b) Exclusive $\pi^+\pi^-$ missing mass with cuts applied to eliminate converted photons and radiative Bhabha events.

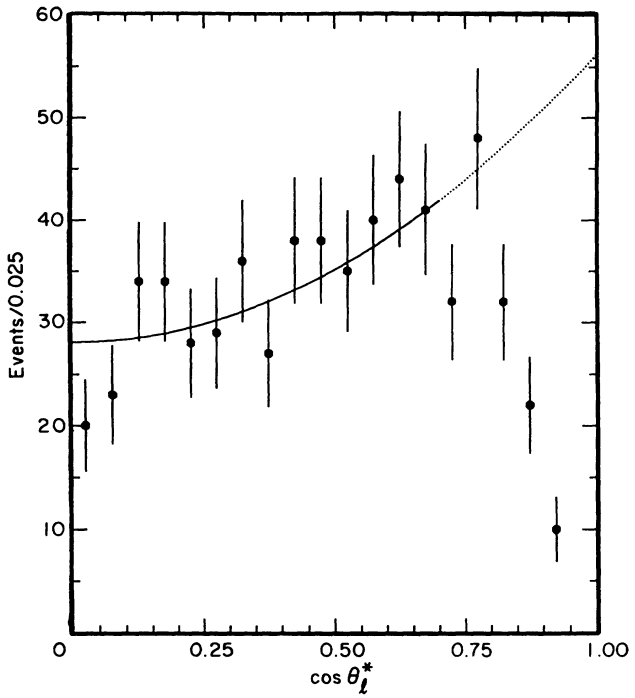

FIG. 8. Uncorrected $\cos\theta_l^*$ distribution of e^+e^- and $\mu^+\mu^-$ pairs from the $\Upsilon(1S)$ from $\Upsilon(3S)\to\pi^+\pi^-\Upsilon(1S)$ decays. The curve shows the fit from a $(1+\cos^2\theta_l^*)$ distribution; events under the dashed line are excluded from the fit and the analysis.

that the daughter $\Upsilon(1S)$ retains the polarization of the parent $\Upsilon(3S)$ along the beam axis. Monte Carlo studies indicate that the lepton finding efficiency is flat in the region $0.0 < |\cos\theta_l^*| < 0.7$.

B. Inclusive event selection

Events in the inclusive analysis are required to pass hadronic selection criteria [36], and must not be consistent with events used in the exclusive analysis. Each candidate transition pion must have momentum less than 750 MeV and specific ionization in the main drift chamber within 3σ of that expected for a pion. We further require these charged tracks to trace back to within 7 cm of the center of the detector along the beam line. The cut on DOCA ranges from 4 to 12 mm, depending on the particle momentum. Tracks associated with a secondary vertex are not used. Figure 9 shows the $\pi^+\pi^-$ recoil mass distribution resulting from this inclusive analysis.

C. $\Upsilon(3S)\to\pi^+\pi^-\Upsilon(1S)$

Figure 10 shows the exclusive and inclusive $\pi^+\pi^-$ missing mass distributions in the $\Upsilon(1S)$ mass region. For the $\Upsilon(3S)\to\pi^+\pi^-\Upsilon(1S)$ decays the faster of the two pions has momentum between 425 and 740 MeV. For the exclusive analysis, we require the DOCA of this pion to be less than 2 mm. Table II shows the total number of events found in the peak, reconstruction efficiency, and branching ratio for the modes studied.

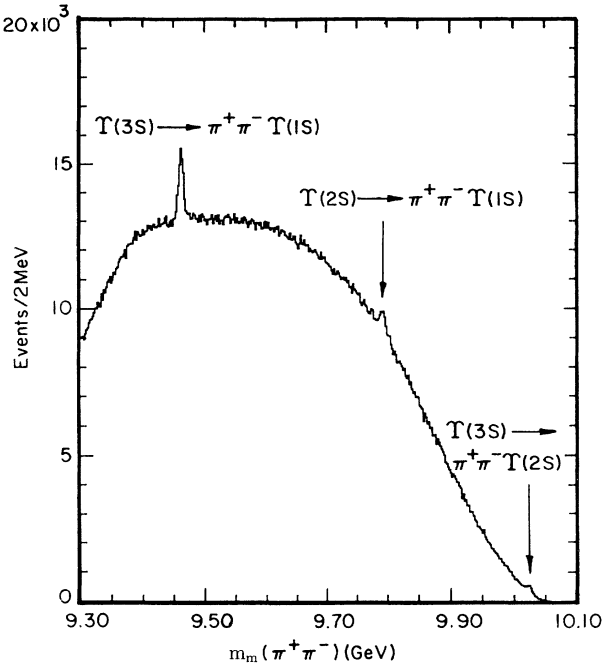

FIG. 9. Inclusive $\pi^+\pi^-$ missing mass spectrum with track quality cuts applied.

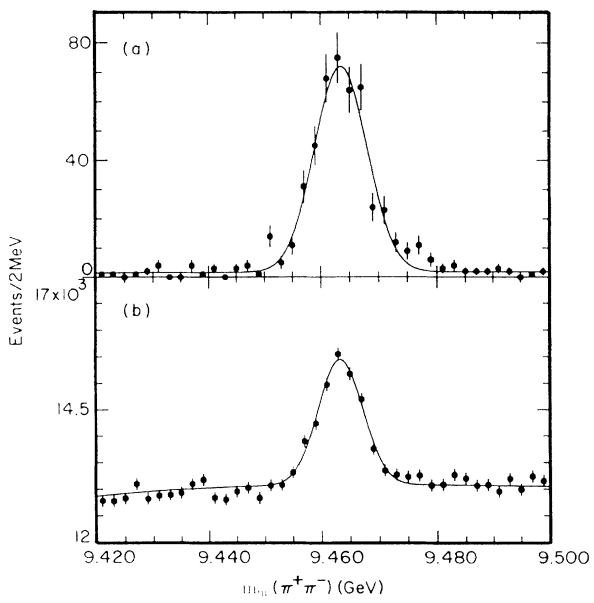

FIG. 10. (a) $\Upsilon(3S)\rightarrow\pi^+\pi^-\Upsilon(1S)$ missing mass peak in the exclusive mode with basic track quality cuts applied to the pion with momentum between 425 and 740 MeV. (b) Inclusive $\pi^+\pi^-$ missing mass distribution in the $\Upsilon(1S)$ mass region (note the suppressed zero in this plot).

Figure 11 shows the $\pi^+\pi^-$ invariant mass distribution for events in the peak region. The simultaneous fit of the exclusive and inclusive data sets to Eq. (6) gives a χ^2/(degree of freedom) of 222/30. The simultaneous fit of the exclusive and inclusive data sets to the Moxhay model gives a χ^2/(degree of freedom) of 32/29, with $\mathrm{Re}(B/A)=0.097\pm0.006$ and $\mathrm{Im}(B/A)=0.284\pm0.003$ [see Eq. (7)], consistent with the values obtained from the $\pi^0\pi^0$ transitions. Another hypothesis to explain the two peak structure of the $\Upsilon(3S)\rightarrow\pi^+\pi^-\Upsilon(1S)$ invariant mass distribution is the coupling of one of the pions and the $\Upsilon(1S)$ to form a resonance. This can easily be tested by examining the invariant mass of the $\pi\Upsilon(1S)$ system. Figure 12 shows the Dalitz plot of $\Upsilon(1S)$ $\pi^+\pi^-$ events. There is no indication in the Dalitz plot of an $\Upsilon(1S)\pi$ resonance.

D. $\Upsilon(3S)\rightarrow\pi^+\pi^-\Upsilon(2S)$

Figure 13 shows the exclusive and inclusive $\pi^+\pi^-$ missing mass distributions in the $\Upsilon(2S)$ mass region. To reduce background levels in the exclusive missing mass distribution we require the opening angle between the pion system and the nearest lepton to be greater than 0.15 radians and the quadratic sum of the impact parameters relative to the beam to be less than 2 cm. Figure 14 shows a candidate $\Upsilon(3S)\rightarrow\pi^+\pi^-\Upsilon(2S)$, $\Upsilon(2S)\rightarrow e^+e^-$ event. Table II shows the total number of events found in the peak, reconstruction efficiency, and branching ratio for this mode.

Figure 15 shows the invariant mass spectrum for pions from $\Upsilon(3S)\rightarrow\pi^+\pi^-\Upsilon(2S)$ decays. The simultaneous fit to the exclusive and inclusive data sets with Eq. (6) gives a χ^2/(degree of freedom) of 20/20.

E. $\Upsilon(3S)\rightarrow\Upsilon(2S)+X$, $\Upsilon(2S)\rightarrow\pi^+\pi^-\Upsilon(1S)$

The $\Upsilon(2S)\rightarrow\pi^+\pi^-\Upsilon(1S)$ branching ratio and $\pi^+\pi^-$ invariant mass shape are already well measured. We therefore use the observed $\Upsilon(2S)\rightarrow\pi^+\pi^-\Upsilon(1S)$ decays

TABLE II. Branching ratios for $\pi^+\pi^-$ transitions.

Decay	Mode	Event count	Efficiency (%)	Branching ratio (%)
$\Upsilon(3S)\rightarrow\pi^+\pi^-\Upsilon(1S)$	Excl.	424±21	39±2.2	4.7±0.2±0.5±0.1
	Incl.	11405±440	58±4	4.4±0.2±0.4
$\Upsilon(3S)\rightarrow\pi^+\pi^-\Upsilon(2S)$	Excl.	55±8	8.9±1.2	$3.2\pm0.5^{+0.7}_{-0.8}\pm0.4$
	Incl.	925±75	7.7±1.8	$2.7\pm0.2^{+0.6}_{-0.7}$
$\Upsilon(3S)\rightarrow\Upsilon(2S)+X$	Excl.	150±13	35.0±2.2	10.0±0.9±1.0±0.5
	Incl.	4475±440	52±4	10.5±1.0±1.1±0.5

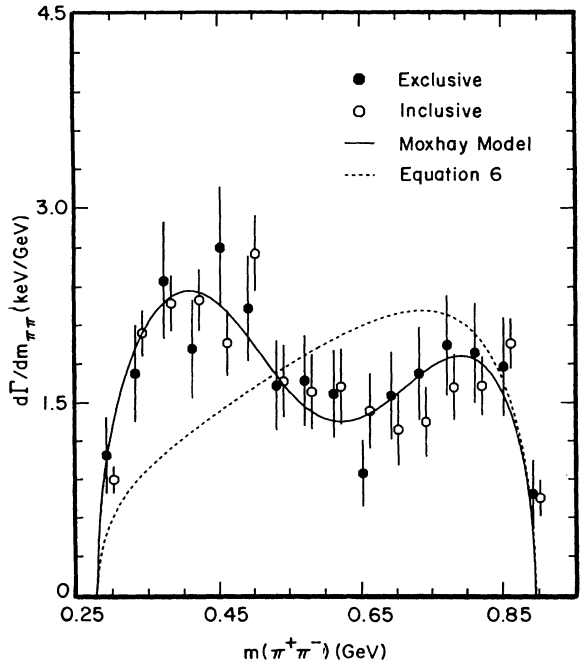

FIG. 11. $\pi^+\pi^-$ invariant mass distribution of pions from $\Upsilon(3S)\to\pi^+\pi^-\Upsilon(1S)$ decays. Simultaneous fits of the exclusive and inclusive distributions to the Moxhay model and Eq. (6) are also shown. The points in the inclusive distribution have been slightly offset from the exclusive points for clarity.

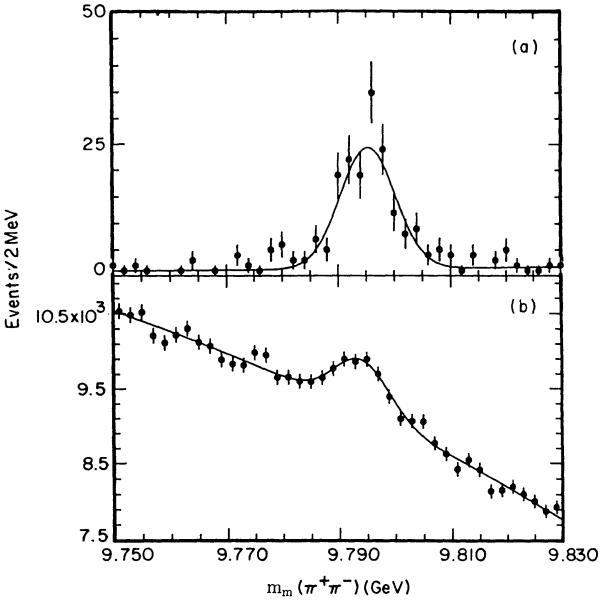

FIG. 13. (a) Exclusive $\pi^+\pi^-$ missing mass distribution in the $\Upsilon(2S)$ mass region. (b) Inclusive $\pi^+\pi^-$ missing mass distribution in the $\Upsilon(2S)$ mass region.

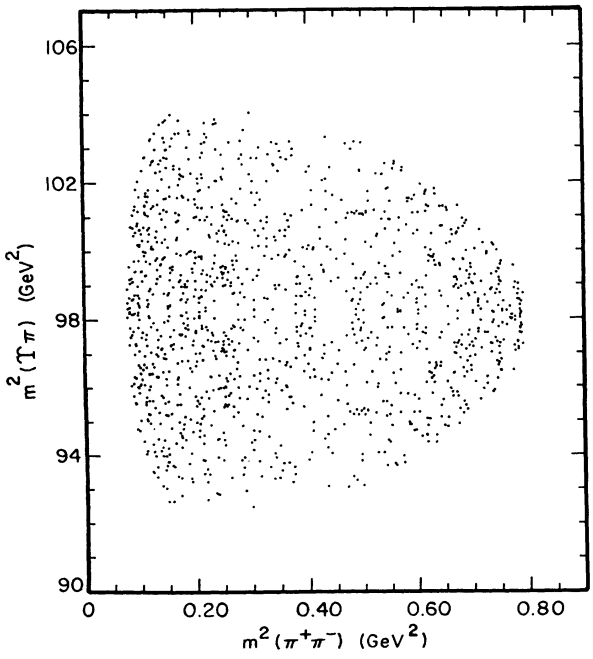

FIG. 12. Dalitz plot for $\Upsilon(3S)\to\pi^+\pi^-\Upsilon(1S)$ decays (two entries per event). The mass squared of $\Upsilon(1S)\pi$ system is plotted against the mass squared of the $\pi^+\pi^-$ system. $M^2_{\Upsilon\pi}$ was calculated with the pion momenta only because the measurement of the pion momenta is superior to the momentum measurements of the much faster leptons.

to measure the branching ratio for $\Upsilon(3S)\to\Upsilon(2S)+X$ where X is either $\pi^+\pi^-$, $\pi^0\pi^0$, or $\gamma\gamma$. Figure 16 shows the exclusive and inclusive missing mass distributions. To reduce background levels in the exclusive missing mass distribution we require the quadratic sum of the DOCA of the two pions to be less than 1 cm and the opening angle of the pion pair to either lepton to be greater than 0.15 radians. The width of the

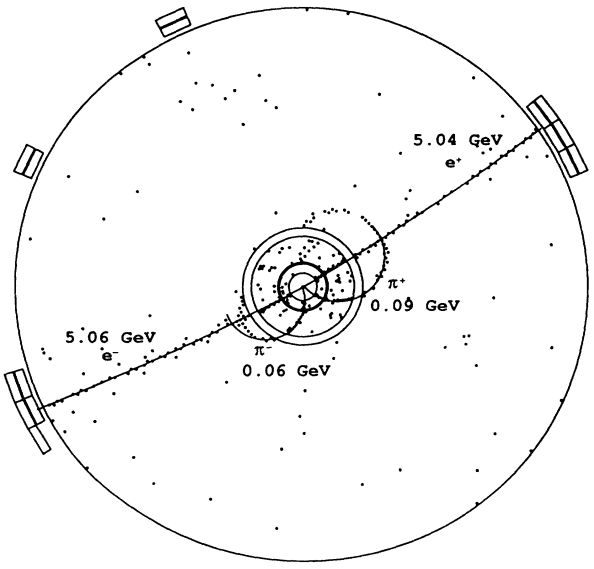

FIG. 14. A candidate $\Upsilon(3S)\to\pi^+\pi^-\Upsilon(2S)$, $\Upsilon(2S)\to e^+e^-$ event. The measured particle momenta (without dE/dx correction) are also displayed. Note how little the slow pions penetrate the main drift chamber.

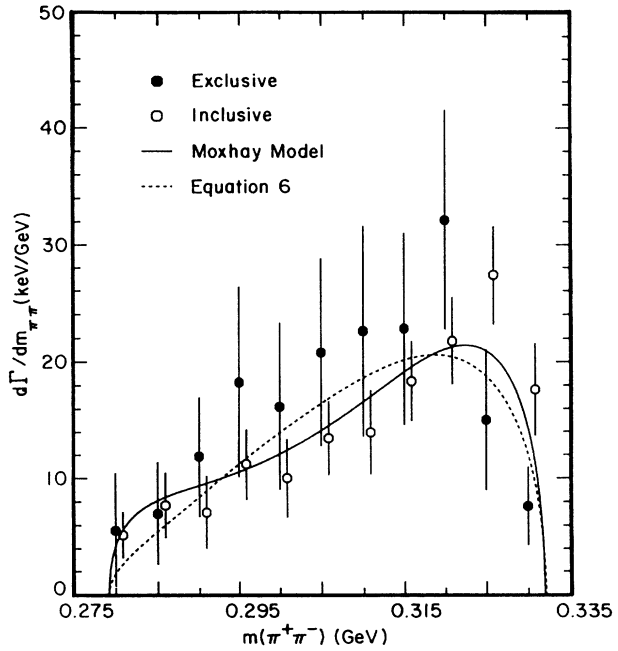

FIG. 15. $\pi^+\pi^-$ invariant mass distribution of pions from $\Upsilon(3S)\to\pi^+\pi^-\Upsilon(2S)$ decays. Simultaneous fits of the exclusive and inclusive distributions to the Moxhay model and Eq. (6) are also shown. The points in the inclusive distribution have been slightly offset from the exclusive points for clarity.

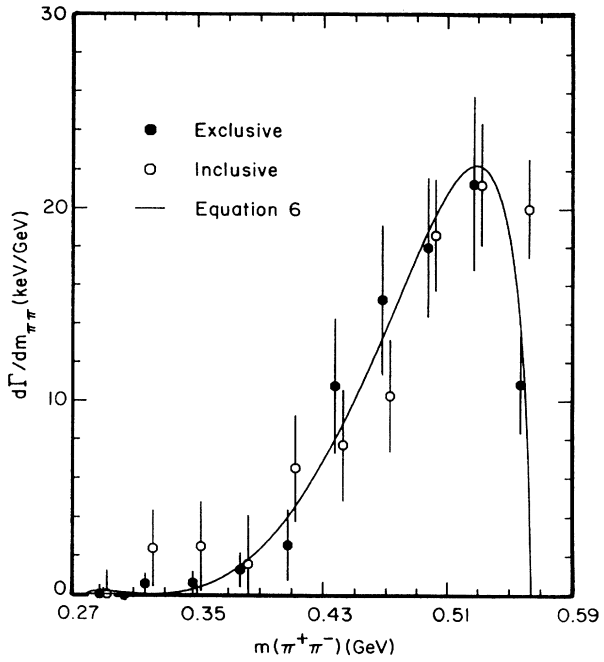

FIG. 17. $\pi^+\pi^-$ invariant mass distribution of pions from $\Upsilon(2S)\to\pi^+\pi^-\Upsilon(1S)$ decays. A simultaneous fit of the exclusive and inclusive distributions to the equation (6) is also shown. The points in the inclusive distribution have been slightly offset from the exclusive points for clarity.

$\Upsilon(2S)\to\pi^+\pi^-\Upsilon(1S)$ peak is Doppler broadened relative to the $\Upsilon(3S)\to\pi^+\pi^-\Upsilon(1S)$ width since the $\Upsilon(2S)$ is recoiling against X in the $\Upsilon(3S)\to\Upsilon(2S)+X$ decay. We tested the sensitivity of the area measurement to changes in the fitting functions (e.g., sum of two Gaussians) [37]. The resulting systematic error is shown in Table IV below. Table II shows the total number of events found in the peak, reconstruction efficiency, and branching ratio for this mode.

Figure 17 shows the $\pi^+\pi^-$ invariant mass distribution for events in the peak region. The simultaneous fit of the exclusive and inclusive data sets to Eq. (6) gives a χ^2/(degree of freedom) of 15/18.

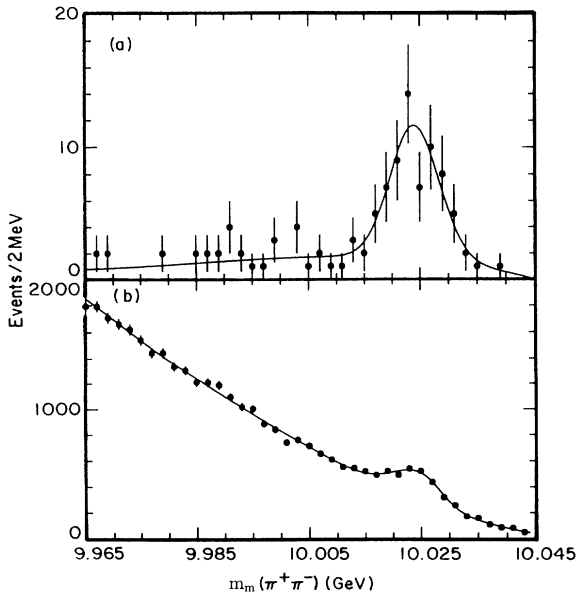

FIG. 16. (a) Exclusive $\pi^+\pi^-$ missing mass in the $\Upsilon(2S)\to\pi^+\pi^-\Upsilon(1S)$ region. (b) Inclusive $\pi^+\pi^-$ missing mass distribution (note the suppressed zero).

F. Branching ratios for $\pi^+\pi^-$ transitions

Table II shows the event count, efficiency, and branching ratio for $\Upsilon(3S)\to\Upsilon(1S)\pi^+\pi^-$, $\Upsilon(3S)\to\Upsilon(2S)\pi^+\pi^-$, and $\Upsilon(3S)\to\Upsilon(2S)+X$ decays for exclusive and inclusive final states. The exclusive efficiencies include trigger efficiencies and a factor of 0.611 from the $|\cos\theta_l|<0.7$ cut. The third mode listed is derived from the cascade decay $\Upsilon(3S)\to\Upsilon(2S)+X$, $\Upsilon(2S)\to\pi^+\pi^-\Upsilon(1S)$. We assume e-μ universality and $\mathcal{B}(\Upsilon(2S)\to\pi^0\pi^0\Upsilon(1S))=\frac{1}{2}\mathcal{B}(\Upsilon(2S)\to\pi^+\pi^-\Upsilon(1S))$. As with the $\pi^0\pi^0$ transitions, the following branching ratios were used to calculate the branching ratios in the table:

$$\mathcal{B}(\Upsilon(1S)\to\mu^+\mu^-)=(2.48\pm0.06)\%\ ,$$

$$\mathcal{B}(\Upsilon(2S)\to\pi^+\pi^-\Upsilon(1S))=(18.5\pm0.8)\%\ ,$$

$$\mathcal{B}(\Upsilon(2S)\to\mu^+\mu^-)=(1.31\pm0.21)\%\ ,$$

and

$$\mathcal{B}(\Upsilon(2S)\to\gamma\gamma\Upsilon(1S))=(3.8\pm0.7)\%\ .$$

The first and second errors on the branching ratios in the table are the statistical and systematic uncertainties respectively. The third error in the branching ratios comes from the uncertainties in the leptonic branching ratios of the $\Upsilon(1S,2S)$ and $\mathcal{B}(\Upsilon(2S)\to\pi^+\pi^-\Upsilon(1S))$.

G. Determination of relative branching fractions by scanning

The low background on the exclusive $\Upsilon(2S)\to\pi^+\pi^-\Upsilon(1S)$ event sample offers an excellent opportunity to study the fraction of $\Upsilon(3S)\to\Upsilon(2S)$ events which are due to $\pi^+\pi^-$, $\pi^0\pi^0$, or $\gamma\gamma$ decays. This allows us to almost eliminate the systematic uncertainties associated with triggering on the events and tracking of the leptons. It also allows us to independently verify the other CLEO measurements of these decays as well as the presumption that the $\pi\pi$ decays are pure $I=0$. Since the quantities of interest here are only relative fractions of the three possible transitions, we do not impose the $\cos\theta_l^*$ cut on the leptons for this part of the analysis.

By scanning the event displays of a sample of $\Upsilon(3S)\to\Upsilon(2S)+X$, $\Upsilon(2S)\to\pi^+\pi^-\Upsilon(1S)$ events, it is possible to visually identify events with 1 or 2 additional slow charged tracks. Many of the events have one additional track at the kinematic limit for charged pions from $\Upsilon(3S)\to\Upsilon(2S)$ decays, while the other pion is too slow to reach the tracking chambers, as shown in Fig. 18. The rest of the events with additional charged tracks show tracks with too low a transverse momentum to give a good total momentum measurement. Monte Carlo studies indicate a 95% efficiency for identifying $\Upsilon(3S)\to\pi^+\pi^-\Upsilon(2S)$ events through this scanning approach.

To determine the number of $\Upsilon(3S)\to\gamma\gamma\Upsilon(2S)$ events we again use a visual scan to identify possible candidates. The efficiency for identifying a $\gamma\gamma$ event candidate from a visual scan is $(84\pm4)\%$, where the efficiency loss is primarily geometric. A separate estimate of the number of $\Upsilon(3S)\to\gamma\gamma\Upsilon(2S)$ events is obtained by examining the photon energy spectrum in the region from 200 to 270 MeV. For increased efficiency and low background we examine the photon energy spectrum in the energy range consistent with the photon from the $\chi(2P)\to\gamma\Upsilon(2S)$ transition. Only photons that are isolated from other showers and not matched to charged tracks are included in the energy spectrum. Figure 19(a) shows the photon energy spectrum with the corresponding fit to the expected photon energies. The fit of the photon energy spectrum gives a yield of 57 ± 11 $\gamma\gamma$ events. The Monte Carlo efficiency for detecting the photon of energy 230 MeV in such events is $(67\pm4)\%$. The final event count is obtained by averaging the two efficiency corrected event counts and is reported in Table III. The spread of the measurements relative to their mean is used as one estimator of the systematic uncertainty.

We similarly determine the $\pi^0\pi^0$ yield by counting π^0's in our tagged $\Upsilon(2S)\to\Upsilon(1S)\pi^+\pi^-$ event sample. Photons considered as candidates for π^0 daughters are required to have energies between 30 and 200 MeV; at least one of the two photons must be within the good barrel re-

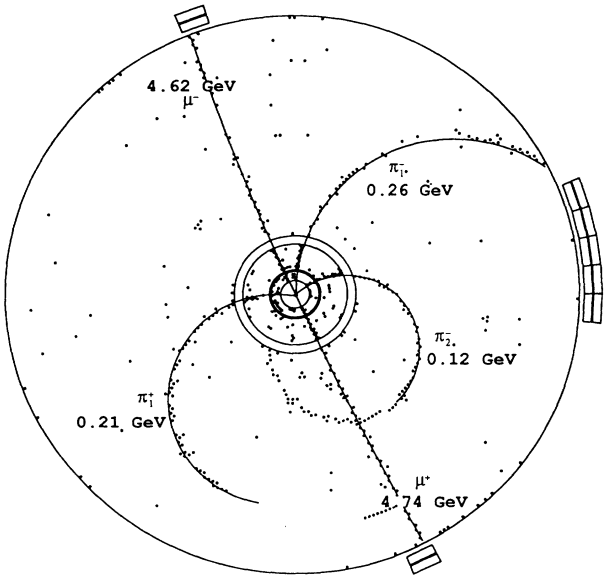

FIG. 18. Candidate $\Upsilon(3S)\to\pi^+\pi^-\Upsilon(2S)$, $\Upsilon(2S)\to\pi^+\pi^-\Upsilon(1S)$ event. The tracks marked π_1^+ and π_1^- have a missing mass consistent with a $\Upsilon(2S)\to\pi^+\pi^-\Upsilon(1S)$ decay. The track marked π_2^- is presumably from a $\Upsilon(3S)\to\pi^+\pi^-\Upsilon(2S)$ decay; we assume the other π^+ failed to penetrate the beam pipe. The measured particle momenta (without dE/dx corrections) are also displayed.

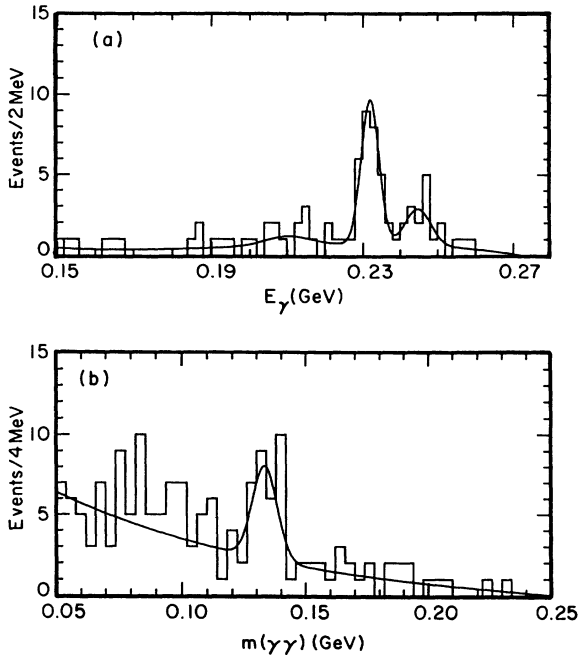

FIG. 19. (a) Photon energy spectrum for events in the $\Upsilon(2S)\to\pi^+\pi^-\Upsilon(1S)$ exclusive missing mass peak. The peaks in the fit have means corresponding to the known photon energies for the $\chi_{bJ}(2P)\to\gamma\Upsilon(2S)$ decays. (b) Two photon invariant mass in the π^0 mass region ($30<E_\gamma<200$ MeV). Photon candidates are required to be isolated and unmatched to charged tracks.

TABLE III. Results of a scan of exclusive $\Upsilon(2S)\to\pi^+\pi^-\Upsilon(1S)$ events.

Mode	Efficiency corrected event count	Relative branching ratio
$\Upsilon(3S)\to\pi^+\pi^-\Upsilon(2S)$	63±9±4	1
$\Upsilon(3S)\to\pi^0\pi^0\Upsilon(2S)$	37±6±4	0.59±0.10±0.07
$\Upsilon(3S)\to\gamma\gamma\Upsilon(2S)$	90±10±6	1.4±0.15±0.13

gion of the calorimeter. Figure 19(b) shows the two photon invariant mass distribution. There are 28±7 π^0's in the peak. The π^0 detection efficiency is (42±6)%. For increased efficiency we do not require both π^0's to be found for each event. Assuming each π^0 in an event can be treated independently, the number of $\pi^0\pi^0$ events in the $\Upsilon(2S)\to\Upsilon(1S)$ peak should be equal to half the efficiency corrected count of π^0's. We also identify $\pi^0\pi^0$ candidates from a visual scan of the data events. Events having two or more low energy showers with at least two low energy showers in the barrel are considered $\pi^0\pi^0$ candidates. The visual scan resulted in a count of 38±6 $\pi^0\pi^0$ events. The efficiency for identifying $\pi^0\pi^0$ candidates from a visual scan of the event displays is (93±8)%. The final event count is obtained by averaging the two efficiency corrected event counts and is reported in Table III.

We have tested the validity of the scan technique using Monte Carlo simulations of $\Upsilon(3S)\to\Upsilon(2S)+X$; $\Upsilon(2S)\to\Upsilon(1S)\pi^+\pi^-$, with the $\Upsilon(1S)$ decaying leptonically. To test the objectivity of the scanner, Monte Carlo events are generated with a mixture of $\pi^+\pi^-$, $\pi^0\pi^0$, and $\gamma\gamma$ that is unknown to the scanner. We find that the physicist doing the scan is able to correctly reproduce the ratio of $\pi^+\pi^-$, $\pi^0\pi^0$, and $\gamma\gamma$ events in the Monte Carlo to within 5%. Thus we have attributed a 5% relative systematic error to possible biases in scanning. Table III shows the efficiency corrected event count for each $\Upsilon(3S)\to\Upsilon(2S)$ decay mode and the branching fractions relative to the number of $\Upsilon(3S)\to\pi^+\pi^-\Upsilon(2S)$ events.

H. Search for $\Upsilon(3S)\to\pi^+\pi^- h_b$

We first search for the h_b in the inclusive $\pi^+\pi^-$ missing mass spectrum (Fig. 9). If the spin-spin interaction is solely responsible for the splitting of the $\chi_b(1P)$ triplet from the singlet, the mass of the h_b should be 9.900 GeV, at the spin-weighted center of gravity of the χ_b triplet. Figure 20 shows the $\pi^+\pi^-$ missing mass in the region around 9.9 GeV. The figure shows a fit to a third-order polynomial and a Gaussian with a mean of 9.900 GeV. The mean of the Gaussian is varied from 9.89 to 9.91 in steps of 1 MeV while the width of the Gaussian is fixed at 3.0 MeV. For values of mean between 9.802 GeV to 9.905 the area of the fit is less than zero. At a missing mass of 9.900 GeV the fitted area of the signal function is −550±170. We therefore take the number of observed events from $\Upsilon(3S)\to\pi^+\pi^- h_b$ transitions to be 0±170. The Monte Carlo efficiency is 33%, giving an upper limit on the inclusive branching ratio for $\Upsilon(3S)\to\pi^+\pi^- h_b$ of 0.18% at 90% confidence level, for $M_{h_b}=9.900$ GeV.

We also search for the h_b in the cascade transition $\Upsilon(3S)\to\pi^+\pi^- h_b$, $h_b\to\gamma\eta_b$. In this search photons are required to be in the barrel region, isolated, and inconsistent with being a photon from a π^0 decay. Monte Carlo studies predict a resolution of 10 MeV on the photon line due to detector resolution. The Lorentz boost of the h_b system is calculated from the known momentum of the two pion system. Knowing the Lorentz boost allows us to recalculate the photon momentum to eliminate the smearing due to Doppler shifting. The $\pi^+\pi^-$ missing mass spectra are found for 32 MeV wide bins in E_γ ($\pm1.6\sigma_{E_\gamma}$). E_γ ranged from 430 to 558 MeV with 8 MeV separation between bin centers. Each missing mass distribution is fit to a Gaussian and a third-order polynomial background. The area of the Gaussian is allowed to float freely, while the h_b mass is restricted to be 9.900±0.003 GeV. The Monte Carlo efficiency for these $\pi^+\pi^-\gamma$ events is (26±4)%.

Figure 21(a) shows the upper limit at 90% confidence level for the product branching ratio for each possible η_b mass. The upper limit for the product branching ratio, assuming an η_b mass of 9.44 GeV, is 0.08%. Figure 21(b)

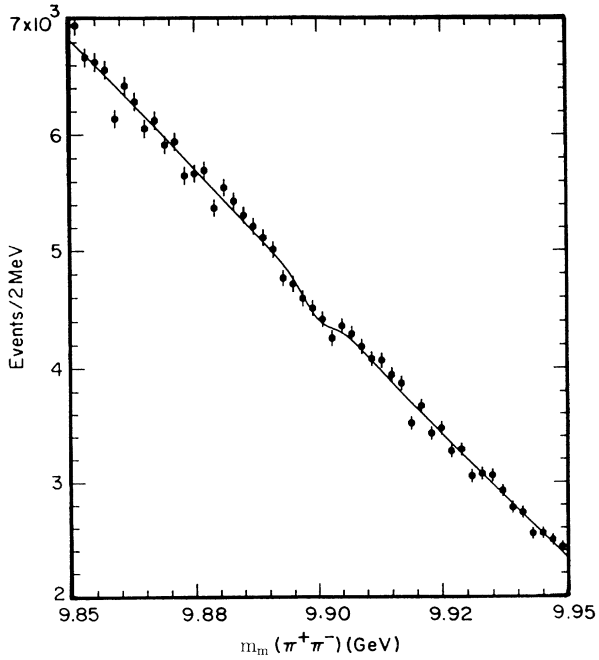

FIG. 20. Inclusive $\pi^+\pi^-$ missing mass distribution in the 9.9 GeV (h_b) mass region.

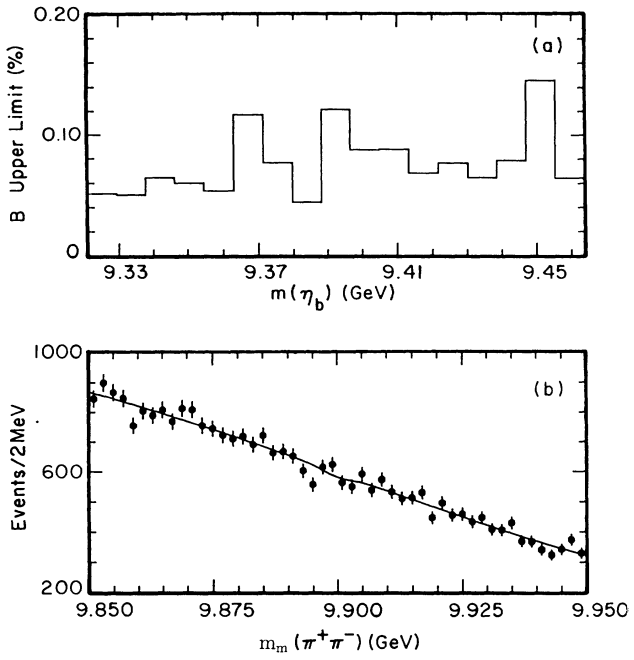

FIG. 21. (a) Upper limit on cascade branching ratio $[\Upsilon(3S)\to h_b\pi^+\pi^-, h_b\to\eta_b\gamma]$ vs η_b mass for 32 MeV slices in E_γ and a missing mass $=9.9$ GeV. (b) $\pi^+\pi^-$ missing mass spectrum for events with a (450 ± 16) MeV photon.

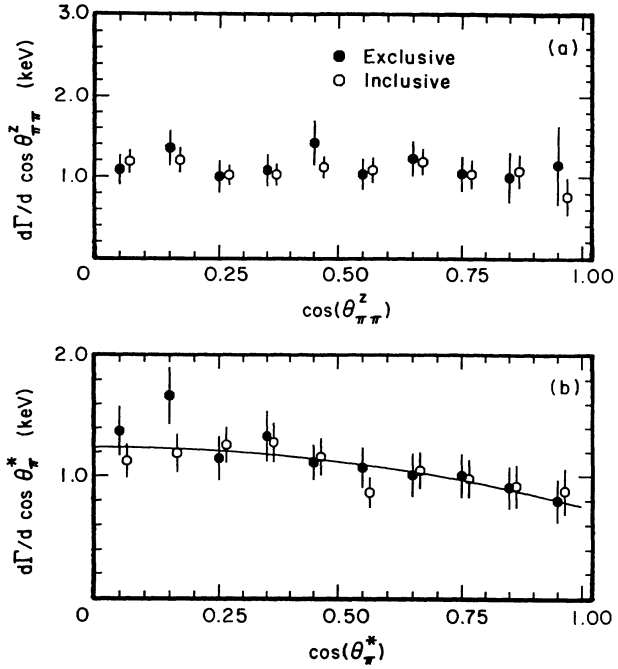

FIG. 22. (a) Efficiency corrected distribution of $\cos\theta^z_{\pi\pi}$, the direction of motion of the $\pi^+\pi^-$ system relative to the beam axis. (b) Efficiency corrected distribution of $\cos\theta^*_\pi$, the π decay angle with respect to the $\pi^+\pi^-$ direction of motion. Also shown is the fit with an $a+b\cos^2\theta$ distribution.

shows the missing mass spectrum for events with a photon with energy between 434 and 466 MeV.

I. Angular distributions of $\pi^+\pi^-$ transitions

In the CESR storage ring, the $\Upsilon(3S)$ is produced with pure transverse polarization along its polarization axis (here, the beam axis). The subsequent decay, $\Upsilon(3S)\to\pi^+\pi^-\Upsilon(1S)$, can proceed with relative angular momentum l between the two pions and/or L of the two pions relative to the $\Upsilon(1S)$. Parity conservation forces these angular momenta to be either both even or both odd and Bose-Einstein statistics and isospin conservation force l (and hence also L) to be even. We find the decay angle distribution of the leptons from the daughter $\Upsilon(1S)$ relative to the beam axis, Fig. 8(a), to be consistent with both $l=L=0$ and $l=L=2$ states.

We have investigated the D_L-wave [38] possibility by considering the distribution of the angle $\theta^z_{\pi\pi}$, defined as the polar angle of the dipion system relative to the beam axis, shown in Fig. 22(a). The $\cos\theta^z_{\pi\pi}$ distribution shows little evidence of being other than a flat distribution. This indicates that the dipion system relative to the $\Upsilon(1S)$ is dominantly in an S_L-wave state. The $\cos\theta^z_{\pi\pi}$ distributions (and the $\cos\theta^*_\pi$ distributions discussed below) are obtained by fitting the dipion missing mass distributions from the $\Upsilon(3S)\to\pi^+\pi^-\Upsilon(1S)$ transitions for each bin of $\cos\theta^z_{\pi\pi}$. The efficiency as a function of $\cos\theta^z_{\pi\pi}$ is obtained in the same manner using Monte Carlo data.

We have also considered the angle θ^*_π, defined as the angle between the π^+ direction in the $\pi^+\pi^-$ center of mass and the $\pi^+\pi^-$ direction of motion in the lab system. The $\cos\theta^*_\pi$ distributions are shown in Fig. 22(b). Performing a simultaneous fit to the efficiency-corrected $\cos\theta^*_\pi$ distributions for $\Upsilon(3S)\to\pi^+\pi^-\Upsilon(1S)$, we obtain an acceptable fit (confidence level of 23%) when we constrain the D_l-wave component to be zero. We obtain a better fit for the case where the magnitude of the D_l-wave amplitude is nonzero. A fit with an $a+b\cos^2\theta^*_\pi$ distribution yields a confidence level of 95% with $a=1.24\pm0.06$ and $b=-0.49\pm0.13$ (statistical errors only). The correlation coefficient between a and b is $\langle\delta a\,\delta b\rangle=-0.76$.

If we assume that the decay is truly S_l wave, and any deviation from uniformity is due to poor detector simulation, this corresponds to an (asymmetric) error of $+10\%$ in our overall $\Upsilon(3S)\to\Upsilon(1S)\pi^+\pi^-$ rate. This error is reported in Table V but is not included in the branching ratios reported in Table III.

For the case of $\Upsilon(3S)\to\pi^+\pi^-\Upsilon(2S)$, where the pion momentum spectrum is much softer, we are prevented from making a statement about any D_l-wave component due to our uncertainty in track-finding efficiency. We therefore assume that the decay is pure S_l wave and determine the change in branching ratio which results from "flattening" our efficiency-corrected $\cos\theta^*$ distribution. This introduces an (asymmetric) error of -15% in our inclusive and exclusive $\Upsilon(3S)\to\pi^+\pi^-\Upsilon(2S)$ branching ratios. This uncertainty is included in the branching ratios reported in Table III.

J. Evaluation of systematic errors

To evaluate our systematic errors, we evaluate the internal consistency of our branching ratios when deter-

TABLE IV. Summary of sources and magnitudes of systematic errors.

	$\pi^+\pi^-\Upsilon(1S)$ (Inclusive)	$\pi^+\pi^-\Upsilon(1S)$ (Exclusive)	$\pi^+\pi^-\Upsilon(2S)$ (Inclusive)	$\pi^+\pi^-\Upsilon(2S)$ (Exclusive)
π^+-finding algorithm			20	20
Event environment	3.7		6.2	
N_{3S}^{pro}	8	8	8	8
ϵ(trigger)		3		5
Fitting function	1	1	1	1
$\frac{S \text{ wave}}{D \text{ wave}}$ in model	+10	+10	−15	−15
$\epsilon_\pi(p_t)$	5	5	4	4

mined in different bins of some parameter. The relative yield between Monte Carlo and data for each transition is calculated as a function of, e.g., transverse momentum of transition pions for exclusive and inclusive events or, e.g., as a function of event multiplicity for the inclusive events. Fluctuations in the yield over transverse momentum or multiplicity indicate systematic differences between the Monte Carlo and data. To estimate the magnitude of the difference, the yields, with their statistical errors, are fit to a constant value using a χ^2 minimization process. If they are consistent at the $\geq 50\%$ confidence level we attribute no systematic error to the observed variations. If the yields are consistent at a confidence level $< 50\%$ we add in quadrature with the statistical error the error required to obtain a confidence level of 50%. We take this additional error to be an estimate of the systematic error. Note that this approach gives a conservative estimate of the systematic error.

For the direct measurements (i.e., all measurements except those based on the visual scan), in addition to the purely statistical errors, there are errors due to uncertainties in track-finding efficiency. We test the sensitivity of the branching ratios to variations in the tracking algorithm used to reconstruct the pions. There are several possible algorithms which can be used to determine the full helical fit to the charged tracks. We have therefore compared the breakdown in both data and Monte Carlo of how the three-dimensional fit was actually done. To evaluate the systematic error, we apply, for both the inclusive and exclusive modes, the $> 50\%$ confidence level criterion described above, using as input the efficiency-corrected branching ratios we obtain when we restrict the type of algorithm which can be used.

For the exclusive case, for which we have made a cut of ≤ 6 tracks in a candidate event, we are susceptible to cases where the tracking algorithm incorrectly reconstructs more than six tracks in a true exclusive event. By examining a sample of seven track events in both data and Monte Carlo, we have found that this effect contributes negligibly to our overall systematic error. For the inclusive case, the multiplicity dependence of the branching ratios we determine allows us to evaluate the dependence on event environment. Note that the fact that the efficiency for reconstructing the two pions in the exclusive mode is higher than for the inclusive mode reflects the greater difficulty of track-finding in a high multiplicity environment. To evaluate the systematic error, we apply, for both the inclusive and exclusive modes, the $> 50\%$ confidence level criterion described above, using as input the branching ratios we obtain when we restrict the allowed multiplicity byte.

To determine the contribution to our apparent $\Upsilon(3S) \rightarrow \Upsilon(2S) + X$ signal from cases where the parent state is something other than the $\Upsilon(3S)$, we have considered the continuum production of $\Upsilon(2S)$ events via the process $e^+e^- \rightarrow \gamma\Upsilon(2S)$. We estimate that $\leq 2\%$ of the $\Upsilon(2S)$ events studied are produced in this manner. We neglect this small effect since the uncertainties on the $\Upsilon(3S) \rightarrow \Upsilon(2S) + X$ branching ratios are approximately 15% for both the exclusive and inclusive modes.

Other additional errors we have considered are uncertainties in dE/dx corrections, absolute trigger efficiency,

TABLE V. Summary of branching ratios and rates of $\pi\pi$ transitions of the $\Upsilon(3S)$.

Mode	Experiment	Branching Ratio (%)	Rates (keV) Result	Zhou-Kang
$\Upsilon(3S) \rightarrow$	CLEO II	1.99±0.34	0.48±0.09±0.06	0.56
$\pi^0\pi^0\Upsilon(1S)$	World Avg.	1.8±0.4		
$\Upsilon(3S) \rightarrow$	CLEO II	4.52±0.35	1.10±0.09±0.13	1.1
$\pi^+\pi^-\Upsilon(1S)$	World Avg.	4.48±0.29		
$\Upsilon(3S) \rightarrow$	CLEO II	2.75±0.7	0.67±0.17±0.08	0.13±0.07
$\pi^0\pi^0\Upsilon(2S)$	World Avg.	1.3±0.4		
$\Upsilon(3S) \rightarrow$	CLEO II	2.9±0.7	0.70±0.17±0.08	0.2±0.1
$\pi^+\pi^-\Upsilon(2S)$	World Avg.	2.1±0.4		
$\Upsilon(3S) \rightarrow$	CLEO II	10.23±1.05	2.43±0.22±0.29	
$\Upsilon(2S)+X$	World Avg.	10.9±1.3		

number of total $\Upsilon(3S)$ hadronic events, and the shape and parameters used to fit the background functions. The complete breakdown of systematic errors is given in Table IV. The entries in the last two rows are correlated since the D-wave component of the amplitude strongly drives the pion momentum spectrum. Errors given are relative errors in percent.

V. DISCUSSION AND CONCLUSIONS

The experimental quantities we measure for the $\Upsilon(3S)\to\pi\pi\Upsilon(1S/2S)$ are the branching ratios, various angular distributions, and the dipion invariant mass distribution. In conjunction with the values of the full width of the $\Upsilon(3S)$ resonance [11], the branching fractions can be used to determine the partial widths for the dipion cascades.

Table V reports the weighted averages of our measurements of the exclusive and inclusive branching ratios for $\Upsilon(3S)\to\pi^+\pi^-\Upsilon(1S,2S)$ transitions, $\Upsilon(3S)\to\Upsilon(2S)+X$ [derived from $\Upsilon(2S)\to\pi^+\pi^-\Upsilon(1S)$], and exclusive branching ratios for $\Upsilon(3S)\to\pi^0\pi^0\Upsilon(1S,2S)$ transitions. These results are compared with previous world averages [11] and the partial rates are compared with those calculated by Zhou and Kuang [25] who have updated and extended the work of Kuang and Yan [13] using the gluon field multipole expansion but also taking into account coupled channel effects. The agreement for $\Gamma(\Upsilon(3S)\to\pi\pi\Upsilon(1S))$ is excellent but possibly accidental because of the drastic disagreement with the $\pi\pi$ effective mass distribution, as discussed below. The calculated $\Gamma(\Upsilon(3S)\to\pi\pi\Upsilon(2S))$ is considerably lower than our result, even taking into account the uncertainty of the calculation.

In conjunction with our previous publication on $\Upsilon(3S)\to\gamma\gamma\Upsilon(2S,1S)$ [39], we have the following measurements.

In the exclusive mode, independent measurements for the $\gamma\gamma$, $\pi^0\pi^0$, and $\pi^+\pi^-$ transitions to the $\Upsilon(2S)$, which we assume saturate the total $\Upsilon(3S)\to\Upsilon(2S)+X$ rate. We express the individual branching ratio measurements as $b_{\gamma\gamma}$, b_{00}, and $b_{\pm}$, respectively. $b_{\pm}$ is from a weighted average of the exclusive and inclusive measurements.

b_X, which is the weighted average of the exclusive and inclusive branching ratio measurements of $\Upsilon(3S)\to\Upsilon(2S)+X$.

From a scan of tagged cascades candidates (C) [the $\Upsilon(3S)\to\Upsilon(2S)+X$, $\Upsilon(2S)\to\Upsilon(1S)\pi^+\pi^-$, $\Upsilon(1S)\to l^+l^-$ events], and using b_X, we have independent determinations of the branching ratios $b^C_{\gamma\gamma}$, b^C_{00}, and $b^C_{\pm}$.

We present a summary of these measurements below. Note that all the branching ratios in Table VI have in common a relative error of 8% due to the uncertainty in the number of $\Upsilon(3S)$ resonance events. This error in the event count is not included in the errors reported in Table VI.

We combine the measurements with correlated systematic errors separately, then take a weighted average of these derived values with each other to determine the single "best" values for the $\gamma\gamma$, $\pi^+\pi^-$, and $\pi^0\pi^0$ cascades to the $\Upsilon(2S)$. The world averages for these transitions are included for comparison [11]. We assume $b_{\gamma\gamma}$, $J=0$, is negligible. These are presented in Table VI.

TABLE VI. CLEO II branching ratios for $\Upsilon(3S)\to\Upsilon(2S)+\gamma\gamma,\pi^0\pi^0,\pi^+\pi^-$.

$b_{\gamma\gamma}(J=2)=1.82\pm0.47$
$b_{\gamma\gamma}(J=1)=3.73\pm0.81$
$b_{\gamma\gamma}(J=0)=<0.45$
$b_{00}=2.76\pm0.77$
$b_{\pm}=3.2\pm0.8$
$b_X=10.2\pm0.9$
$b^C_{\gamma\gamma}=4.83\pm0.76$
$b^C_{00}=1.99\pm0.43$
$b^C_{\pm}=3.38\pm0.61$

Isospin conservation requires the $\pi\pi$ system to be in an $I=0$ state in all of these transitions. The square of the matrix elements for the $\pi^+\pi^-$ transitions should then be double those for the $\pi^0\pi^0$ transitions. The branching ratios also depend on the available phase space which is larger for the $\pi^0\pi^0$ transitions. The ratios of available phase spaces $(\pi^0\pi^0/\pi^+\pi^-)$ is 1.36 for $\Upsilon(3S)\to\pi^0\pi^0\Upsilon(2S)$ and 1.02 for $\Upsilon(3S)\to\pi^0\pi^0\Upsilon(1S)$. [The increase in the available phase space is more pronounced in the $\Upsilon(3S)\to\pi^0\pi^0\Upsilon(2S)$ because this transition is close to the threshold.] Taking into account these phase space factors, we expect the ratio $\mathcal{B}(\Upsilon(3S)\to\pi^0\pi^0\Upsilon(1S))/\mathcal{B}(\Upsilon(3S)\to\pi^+\pi^-\Upsilon(1S))$ to be 0.51, we find 0.44 ± 0.07 [the common relative error of 8% for the number of $\Upsilon(3S)$ events has been accounted for]. For the ratio $\mathcal{B}(\Upsilon(3S)\to\pi^0\pi^0\Upsilon(2S))/\mathcal{B}(\Upsilon(3S)\to\pi^+\pi^-\Upsilon(2S))$ we expect 0.68 and the analogous comparison yields 0.69 ± 0.17.

We note generally good consistency between all the CLEO-II measurements. Taking into account phase space considerations, agreement with the assumption that the $\pi\pi$ system is produced in an isospin $I=0$ state is very good for both the $\Upsilon(3S)\to\Upsilon(2S)\pi\pi$ and $\Upsilon(3S)\to\Upsilon(1S)\pi\pi$ transitions.

We observe no indications of the $h_b(9900)$, and have set limits comparable to the CLEO 1.5 limits. We have also set upper limits for the isospin-violating decay: $\Upsilon(3S)\to\pi^0h_b$, at a level of sensitivity which is still lower than model predictions.

We have measured angular distributions of the final state particles in our decays. The distribution of the final state leptons in the (exclusive) $\Upsilon(3S)$

TABLE VII. Branching ratios for $\Upsilon(3S)\to\Upsilon(2S)+\gamma\gamma,\pi^0\pi^0,\pi^+\pi^-$.

Mode	CLEO II (%)	Previous World Avg. (%)
$\Upsilon(3S)\to\gamma\gamma\Upsilon(2S)$	5.02 ± 0.69	4.7 ± 1.04
$\Upsilon(3S)\to\pi^0\pi^0\Upsilon(2S)$	2.16 ± 0.39	1.3 ± 0.4
$\Upsilon(3S)\to\pi^+\pi^-\Upsilon(2S)$	3.12 ± 0.49	2.1 ± 0.4

$\rightarrow\Upsilon(1S)\pi^+\pi^-\rightarrow l^+l^-\pi^+\pi^-$ sample, where our statistics are the highest, is consistent with being entirely $(1+\cos^2\theta_l^*)$. This is expected for an S-wave decay, or a D-wave decay where the component of spin along the polarization axis (here, the beam axis) is zero or two. Further examination of our data suggests that there may be partial $\pi\pi$ waves higher than the S_l wave in the transition $\Upsilon(3S)\rightarrow\Upsilon(1S)\pi^+\pi^-$, as inferred from the helicity angle distribution of the $\pi^+\pi^-$ system. However, due to the difficulties in modeling the momentum dependence of the $\pi^\pm$ detection efficiency and to the ineluctable dependence of reconstruction efficiency on dipion mass, this is a study which awaits larger data samples for completion.

The dipion mass distributions we observe for $\Upsilon(3S)\rightarrow\pi\pi\Upsilon(2S)$ are consistent with the multipole expansion model where the model purports to be most reliable. However the extremely narrow range of dipion mass in this decay makes conclusions about the shape rather unreliable.

The $\pi^0\pi^0$ and $\pi^+\pi^-$ invariant mass distributions in the $\Upsilon(3S)\rightarrow\pi\pi\Upsilon(1S)$ transition confirm the double bump structure that disagrees with the gluon field multipole expansion model [20,21], as well as the expectation that the matrix element for a transition with these quantum numbers should approach zero at threshold (the so-called "Adler zero"). This is perhaps an indication that the average value of Q^2 is too large to reliably make predictions using the multipole model. It finds an acceptable interpretation in the interference of the multipole expansion amplitude with a simple parametrization (just a complex constant) of an amplitude due to intermediate $B\bar{B}^*$ states [23,24]. However Zhou and Kuang [25], explicitly calculating coupled channel effects, have shown that this interpretation is not acceptable, but their $\pi\pi$ mass distribution disagrees strongly with the data. The dynamics governing this transition remains a mystery.

ACKNOWLEDGMENTS

We gratefully acknowledge the effort of the CESR staff in providing us with unequaled luminosity and running conditions. J.P.A. and P.S.D. thank the PYI program of the NSF; I.P.J.S. thanks the YI program of the NSF; K.H. thanks the Alexander von Humboldt Stiftung; G.E. thanks the Heisenberg Foundation; K.K.G. and A.J.W. thank the SSC Fellowship program of TNRLC; K.K.G., H.N.N., J.D.R., and H.Y. thank the OJI program of DOE; and R.P. and P.R. thank the A.P. Sloan Foundation for support. This work was supported by the National Science Foundation and the U.S. Dept. of Energy.

[1] See, e.g., W. Kwong, J. L. Rosner, and C. Quigg, Annu. Rev. Nucl. Part. Sci. **37**, 325 (1987).
[2] For a review, see M. B. Voloshin and Yu. M. Zaitev, Usp. Fiz. Nauk **152**, 361 (1987) [Sov. Phys. Usp. **30**, 553 (1987)].
[3] ARGUS Collaboration, H. Albrecht *et al.*, Phys. Lett. **160B**, 331 (1985).
[4] ARGUS Collaboration, H. Albrecht *et al.*, Z. Phys. C **35**, 283 (1987).
[5] CLEO Collaboration, I. C. Brock *et al.*, Phys. Rev. D **43**, 1448 (1991).
[6] CLEO Collaboration, R. Morrison *et al.*, Phys. Rev. Lett. **67**, 1696 (1991).
[7] Crystal Ball Collaboration, R. Nernst *et al.*, Phys. Rev. Lett. **54**, 2195 (1985).
[8] CUSB Collaboration, U. Heintz *et al.*, Phys. Rev. Lett. **66**, 1563 (1991).
[9] CUSB Collaboration, Q. Wu *et al.*, Phys. Lett. B **301**, 307 (1993).
[10] CUSB Collaboration, M. Narain *et al.*, Phys. Rev. Lett. **66**, 3113 (1991).
[11] For earlier references, see Particle Data Group, K. Hikasa *et al.*, Phys. Rev. D **45**, S1 (1992).
[12] K. Gottfried, in *Proceedings of the International Symposium on Lepton and Photon Interactions at High Energies,* Hamburg, 1977, edited by F. Gutbrod (DESY, Hamburg, 1977), p. 667; Phys. Rev. Lett. **40**, 598 (1978).
[13] Y. P. Kuang and T. M. Yan, Phys. Rev. D **24**, 2874 (1981).
[14] M. B. Voloshin, Nucl. Phys. **B154**, 365 (1979); M. B. Voloshin and V. Zakharov, Phys. Rev. Lett. **45**, 688 (1980).
[15] V. A. Novikov and M. A. Shifman, Z. Phys. C **8**, 43 (1981).
[16] D. Morgan and M. R. Pennington, Phys. Rev. D **12**, 1283 (1975).
[17] L. S. Brown and R. N. Cahn, Phys. Rev. Lett. **35**, 1 (1975).
[18] M. B. Voloshin, Pis'ma Zh. Eksp. Teor. Fiz. **21**, 733 (1975) [JEPT Lett. **21**, 347 (1975)].
[19] T. N. Pham, B. Pire, and T. N. Truong, Phys. Lett. **61B**, 183 (1976); Phys. Rev. D **13**, 620 (1976).
[20] T. M. Yan, Phys. Rev. D **22**, 1652 (1980).
[21] G. Bélanger, T. DeGrand, and P. Moxhay, Phys. Rev. D **39**, 257 (1989).
[22] M. B. Voloshin, Pis'ma Zh. Eksp. Teor. Fiz. **37**, 58 (1983) [JETP Lett. **37**, 69 (1983)].
[23] H. J. Lipkin and S. F. Tuan, Phys. Lett. B **206**, 349 (1988).
[24] P. Moxhay, Phys. Rev. D **39**, 3497 (1989).
[25] H.-Y. Zhou and Y.-P. Kuang, Phys. Rev. D **44**, 756 (1991).
[26] K. Heikkila, S. Ono, and N. A. Törnqvist, Phys. Rev. D **29**, 110 (1984); S. Ono and N. A. Törnqvist, Z. Phys. C **23**, 59 (1984); N. A. Törnqvist, Phys. Rev. Lett. **53**, 878 (1984); Acta Phys. Pol B **16**, 503 (1985).
[27] A. Le Yaouanc, L. Oliver, O. Pène, and J.-C. Raynal, Phys. Rev. D **8**, 2223 (1973).
[28] E. Eichten *et al.*, Phys. Rev. D **17**, 3090 (1978); **21**, 313(E) (1980); **21**, 203 (1980).
[29] CLEO Collaboration, Y. Kubota *et al.*, Nucl. Instrum. Methods **A320**, 66 (1992).
[30] D. G. Cassel *et al.*, Nucl. Instrum. Methods **A252**, 325 (1986).
[31] E. Blucher *et al.*, Nucl. Instrum. Methods **A249**, 201 (1989).
[32] D. Bortoletto *et al.*, Nucl. Instrum. Methods **A320**, 114 (1992).
[33] R. Brun *et al.*, GEANT 3.14, Report No. CERN DD/EE/84-1, 1984 (unpublished).
[34] H. Albrecht, Z. Phys. C **35**, 283 (1987).
[35] The Monte Carlo simulation shows that the resolution for

the $\pi^0\pi^0$ invariant mass is better than the bin size.

[36] The hadronic event selection criteria are (1) a minimum of three charged tracks in the event, (2) the total energy of the event must be greater than 15% of the center-of-mass energy of the beams, (3) the event vertex must be within 2 cm of the nominal beam crossing position in the r-ϕ plane, and (4) the z vertex position of the event must be within 5 cm of nominal beam crossing position.

[37] Recall that the $\Upsilon(2S)$ can be reached from the $\Upsilon(3S)$ via two pion decay or two photon decay. Each mode results in a different amount of smearing of the recoil mass measurement. However, the difference in Doppler smearing is small and the detector resolution also widens the distribution and obscures the effect of having two different Gaussians.

[38] Both $L=2$ and $l=2$ can be referred to as D-wave states. We will refer to the $L=2$ state as D_L wave and the $l=2$ state as D_l wave to remove the ambiguity.

[39] CLEO Collaboration, G. Crawford *et al.*, Phys. Lett. B **294**, 139 (1992).

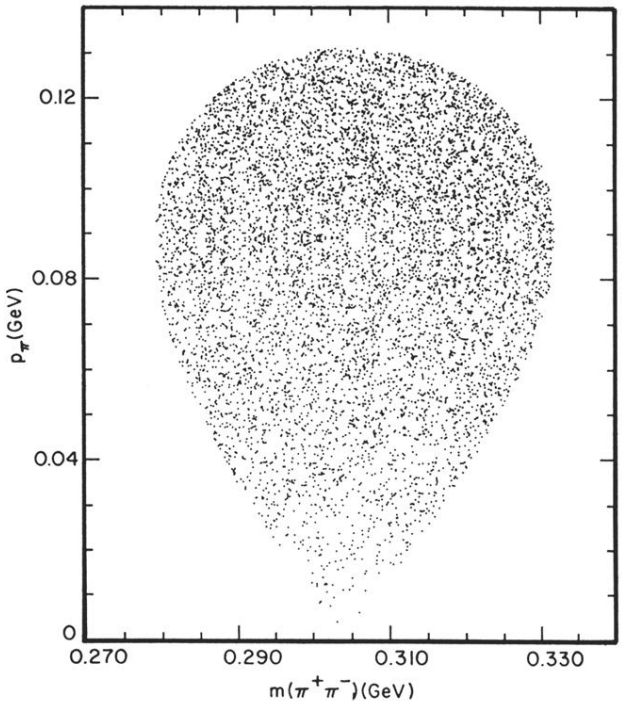

FIG. 6. Scatter plot of charged pion momentum vs $\pi^+\pi^-$ invariant mass (two entries per event) for $\Upsilon(3S) \rightarrow \pi^+\pi^-\Upsilon(2S)$ using our Monte Carlo generator for this process.